Received: 6 September 2024 | Revised: 24 March 2025 | Accepted: 2 April 2025

DOI: 10.1002/qj.4995

Quarterly Journal of the Royal Meteorological Society RMetS

RESEARCH ARTICLE

Modulations of local rainfall in northeast Australia associated with the Madden–Julian oscillation during austral summer

Thi Lan Dao[1,2] | **C. L. Vincent**[1,2] | **Y. Huang**[1,2] | **J. S. Soderholm**[3]

[1]School of Geography, Earth and Atmospheric Sciences, The University of Melbourne, Melbourne, Victoria, Australia

[2]ARC Centre of Excellence for the Weather of the 21st Century,

[3]Science and Innovation Group, The Bureau of Meteorology, Melbourne, Victoria, Australia

Correspondence
Thi Lan Dao, School of Geography, Earth and Atmospheric Sciences, The University of Melbourne, VIC, Australia.
Email: thiland@student.unimelb.edu.au

Funding information
Australian Research Council (ARC) Centre of Excellence for the Weather of the 21st Century, Grant/Award Number: CE230100012; Melbourne Research Scholarship; Rowden White Scholarship

Abstract

This study investigates the role of the interaction between the Madden–Julian oscillation (MJO) and local-scale forcings in regulating precipitation and its diurnal variation during the austral summer over coastal areas in northeast (NE) Australia using radar data. The variation of rainfall is influenced by both large-scale and local-scale forcings. During the enhanced convection phases of the MJO, widespread increased rainfall signals are generated by large-scale forcings associated with the MJO, but the environmental factors controlling the type and amount of precipitation during each phase are different. By contrast, the locally enhanced rainfall during suppressed convection phases of the MJO likely results from the interaction of mesoscale land–sea breezes, strong large-scale background winds and topography. Different responses of mean and heavy precipitation to the MJO occur in some MJO phases. The impact of the MJO on diurnal rainfall characteristics is spatially inhomogeneous and likely regulated by local forcings. Although stratiform rainfall is more common, convective rainfall predominantly contributes to the total precipitation over coastal regions of NE Australia. The MJO's influence on convective rainfall is generally stronger and more statistically significant than its impact on stratiform rainfall. The widespread increased rainfall probability during the enhanced convection phases is likely due to increases in both stratiform and convective rainfall. In contrast, the locally enhanced precipitation signal during some suppressed convection phases mainly results from an increase in convective rainfall.

KEYWORDS

coastal rainfall, extreme rainfall, MJO, radar data, scale interactions

1 | INTRODUCTION

The Madden–Julian oscillation (MJO), characterized by a planetary-scale eastward propagation of rainfall and the associated atmospheric circulation, is recognized as the dominant mode of intraseasonal variability in the tropics (Madden & Julian, 1971, 1972). Numerous studies have shown that the MJO strongly affects both tropical and

extratropical precipitation in Australia (Cowan et al., 2023; Dao et al., 2023; Marshall et al., 2021; Wheeler et al., 2009; Wheeler & Hendon, 2004). In the austral summer season, northern Australia rainfall is significantly enhanced when the MJO convection arrives in the Maritime Continent and western Pacific, and suppressed when the MJO convection occurs in the western Indian Ocean and Africa (Ghelani et al., 2017; Wheeler et al., 2009). The MJO also affects Australia's extratropical precipitation by remotely modulating extratropical circulations (Matthews et al., 2004) and this indirect influence could occur even without a direct MJO impact in tropical Australia (Marshall et al., 2021). In addition to mean rainfall, extreme rainfall events are also regulated by the MJO with a higher chance of extreme precipitation occurring during the enhanced convection phases of the MJO (Dao et al., 2023; Marshall et al., 2021; Schreck III, 2021).

Impacts of the MJO on the diurnal cycle of precipitation have previously been investigated using different datasets such as reanalysis, satellite or radar data. For example, the Tropical Rainfall Measuring Mission (TRMM) 3B42 has been widely used to examine the MJO-related rainfall diurnal variation over the Maritime Continent (Ling et al., 2019; Peatman et al., 2014; Rauniyar & Walsh, 2011; Vincent & Lane, 2016). Over the Maritime Continent, precipitation peaks over land before the active convection phases of the MJO arrive and decreases when the MJO convention centre resides over the region (Birch et al., 2016; Oh et al., 2012; Qian, 2020; Rauniyar & Walsh, 2011). Using the geostationary satellite Himawari-8, Lopez-Bravo et al. (2023) showed that the MJO affects the diurnal cycle of precipitation and deep convective clouds over Sumatra and adjacent ocean. Rowe et al. (2019) pointed out that the occurrence time of radar-derived rainfall is influenced by synoptic-scale equatorial waves during MJO enhanced phases. Using observations from a C-band Doppler radar, Lestari et al. (2022) investigated the local mean and extreme subdaily rainfall response to the MJO in Jakarta. Their findings suggest that high-resolution radar observations allow for better characterization of the timing and likelihood of local heavy rainfall and their interaction with the MJO.

Radar data have also been utilized to investigate the rainfall characteristics associated with the MJO. Powell and Houze Jr. (2013), using radar observations from the Atmospheric Radiation Measurement Madden–Julian Investigation Experiments field campaigns, found that stratiform precipitation increases with the onset of the MJO, while convective rainfall becomes more common in the days preceding the MJO onset over the Indian Ocean. Similarly, previous studies using the TRMM precipitation radar showed that rainfall is more convective before the MJO onset and more stratiform once the MJO reaches the Maritime Continent (Bai, 2021; Vincent & Lane, 2018). Additionally, Alber et al. (2023) discovered that the MJO has a stronger impact on the diurnal cycle of stratiform rainfall compared to convective rainfall over the Congo basin. In Australia, radar data have also been applied to understand mean and heavy-rainfall characteristics in a number of studies. For instance, C-band polarimetric (CPOL) radar data were used to understand several characteristics of convective precipitation and its diurnal cycle over Darwin, Australia (Kumar et al., 2013; May et al., 2012). Hitchcock et al. (2021) examined the features of linear rainfall systems and their relationship to heavy precipitation over Melbourne using the Australian Radar Archive dataset. Ayat et al. (2023) also used the same dataset to understand the climatological characteristics of rainfall system in Sydney, Australia. However, only a few studies (Rauniyar & Walsh, 2016) have used radar data to investigate the variation of local precipitation with large-scale climate modes, in part because few radar datasets are long enough to sample multiple phases of multiyear climate modes.

Recent studies have highlighted the role of topography in modulating local precipitation under the backdrop of MJO. For example, Wei et al. (2020) found that the variation of the rainfall diurnal cycle with the MJO over the Maritime Continent changes among islands depending on their size and topography. Lestari et al. (2022) also demonstrated that although the MJO exerts a significant impact on the rain rate in Jakarta, its impact is further modulated by topography. Another mesoscale process affecting the local rainfall and its diurnal cycle is the land–sea breeze circulation. The connection between rainfall and land–sea breeze circulation over the Maritime Continent is found to vary with coastline orientation and background wind (Short et al., 2019). Stronger sea breezes are often associated with an enhanced diurnal cycle of rainfall during suppressed convection phases of the MJO over the Maritime Continent (Birch et al., 2016; Peatman et al., 2014; Vincent & Lane, 2017; Wei et al., 2020). By examining the thermal contrast between land and sea, Rauniyar and Walsh (2016) found weaker sea breezes during active MJO phases compared to suppressed MJO phases over Darwin and its surrounding areas. The variation in land–sea circulation with MJO phases can be due to changes in the shortwave radiation received at the surface, changes in background wind and changes in vertical structure of potential temperature. May et al. (2012) found that the surface receives approximately 40% of the clear-sky solar radiation amount during enhanced convection phases and around 80% during suppressed convection phases of the MJO over Darwin, Australia. Although the relationship between the MJO and land–sea breezes has been extensively studied in the deep

tropics, how this relationship changes in the subtropics is not well understood.

Northeast (NE) Australia, extending from the deep tropics to subtropics, is often subjected to heavy-rainfall events such as 2010–2011 Queensland floods (King et al., 2013), the 2019 Townsville flood (Cowan et al., 2019), the 2022 Eastern Australia floods (Goodwin, 2022), and the 2023 Cairns floods (Davies, 2024). This important agricultural area where more than 95% of Australia's sugarcane is grown (Smith et al., 2014), is characterized by complex topography including the Great Dividing Range (GDR) with many mountain ranges and plateaus. The GDR affects rainfall distributions and the movement of fronts and other weather phenomena, resulting in inhomogeneous precipitation patterns between the two sides of the mountains (Black & Lane, 2015; Pepler et al., 2020; Twomey & Kiem, 2021). The interactions of these local features with large-scale climate modes may produce different influences on mean and heavy precipitation in this region. Dao et al. (2023) examined multiscale influences on precipitation in NE Australia using station-based gridded data (AGCD) and TRMM 3B42 satellite data. They found that the impacts of the MJO on rainfall and its diurnal cycle reveal a marked geographical variation and that coarse-resolution datasets cannot capture well the topographic/coastal features of the precipitation response. Their study also suggests that higher-resolution observational data such as weather radar or high-density station network are needed to understand the spatial distribution and diurnal timing of rainfall as well as its interaction with large-scale climate variability.

While previous studies have discussed the influences of the MJO on rainfall and its diurnal cycle, how these impacts are modulated by local forcings remains unclear. In addition, it is also important to improve the understanding of the timing and amplitude of rainfall diurnal peaks using high-resolution subdaily observations. This study aims to examine the interaction of the MJO with local forcings associated with topography, coastal processes, and convection in regulating precipitation and its diurnal variation over coastal areas in NE Australia using weather radar data. The study focuses on two modern S-band Doppler radars at Brisbane and Townsville (Figure 1), which reside in the coastal area of Queensland where strong influences of both intraseasonal scales and local circulations such as the land–sea breezes are expected. The two selected radars represent distinct geographic locations, each of which can be modulated differently by the MJO. Precipitation at the cTownsville radar can be modulated by both direct and indirect effects of the MJO, while the Brisbane radar is

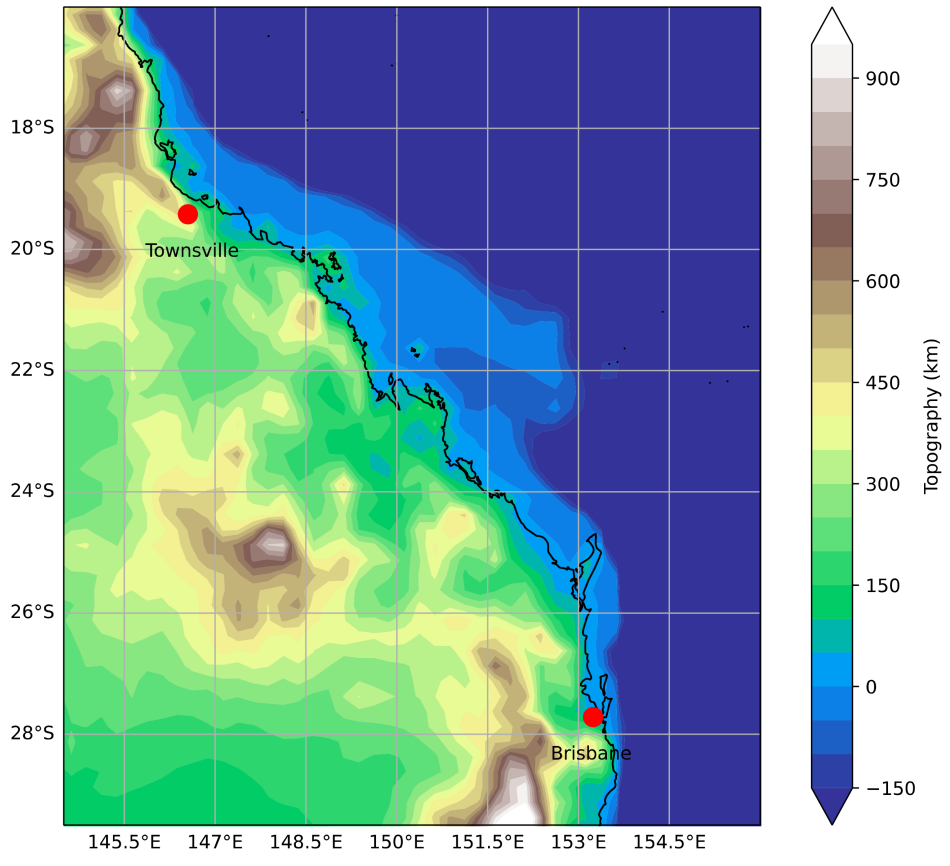

FIGURE 1 Bathymetric map with location and radius coverage of the two radars used in this study. [Colour figure can be viewed at wileyonlinelibrary.com]

located over the subtropical region that could be affected by the remote impacts of the MJO. We address three key questions in this study: (1) how does the radar-derived mean and heavy rainfall vary with MJO phases over the coastal regions of Queensland? (2) How do the timing and amplitude of rainfall diurnal variability vary under different MJO phases? (3) How do radar-observed rainfall characteristics (convective/stratiform rainfall) change with MJO phase? The remainder of this paper is organized as follows. Data and methods are presented in Section 2. Section 3 discusses the variations of mean, heavy, diurnally varying rainfall and convective/stratiform rainfall to the MJO. The possible mechanisms responsible for the observed precipitation patterns are discussed in Section 4. Discussions and conclusions are summarized in Sections 5.

2 | DATA AND METHODS

2.1 | Radar dataset

Rainfall data employed in this study are from the Australian Operational Weather Radar dataset (Soderholm et al., 2022), which has previously been applied in several studies to investigate the rainfall characteristics in Australia (e.g., Ayat et al., 2023; Hitchcock et al., 2021). The full dataset contains observations obtained from 76 radars across Australia (including polarimetric radars), and many sites have more than 20 years of data. The level-2 dataset provides several retrieved variables including estimates of rain rate and a convective/stratiform classification, with a spatial resolution of 1 km out to a range of 150 km from the radar location. All analyses are performed for the period from 01/12/2011 to 28/02/2022 focusing on the austral summer season (DJF). This 11-year period is selected based on the data availability for both the Townsville and Brisbane radars.

Both radars have a one-degree beam width, 250-m range gates and complete the same volume scanning pattern of 14 tilts within 6 min. The calibration of radar reflectivity at each site is first corrected using a volume-matching technique described by Louf et al. (2019) that compares ground radar with satellite radar samples. The calibration is performed against the Global Precipitation Measurement (GPM) precipitation radar for the period March 2014 to present, and the TRMM precipitation radar prior to this date. Ground clutter is removed first by the radar signal processing and second as part of post-processing using the echo area and continuity filter (Gabella & Notarpietro, 2002). These filtering steps remove most of the ground clutter; however, given the radars used in this study lack dual-polarized measurements for the entire duration of the analysis period, it is difficult to completely remove all ground clutter. Next, reflectivity data are interpolated from radar coordinates to mapping coordinates using the technique described by Dahl et al. (2019), which applies Cressman interpolation (with a 2.5 km radius of influence) in the horizontal and nearest-neighbour interpolation in the vertical. The interpolated grid has a resolution of 1 km in the horizontal and 0.5 km in the vertical. From these 3D gridded data, the horizontal slice at 2.5 km above mean sea level is extracted for applying the convective–stratiform classification and the lowest valid grid value below 2.5 km is extracted for applying the reflectivity–rain rate (Z–R) relationship. The Z–R relationships (Table 1) were developed by fitting lowest valid reflectivity samples to the nearby (2 to 75 km radius of each radar) rain gauge measurements. Areas where the radar signal is mostly blocked have been removed using rainfall thresholds for both radars, corresponding to the missing sectors in Figures 2 to 9.

The convective and stratiform precipitations are classified using the algorithm developed by Raut et al. (2020). The algorithm first converts radar reflectivity to rainfall and then classifies the convective and stratiform regions using wavelet scale analysis. The à trous wavelet transform is applied to separate the inhomogeneous convective rainfall from relatively smooth stratiform rainfall. The inhomogeneous region is further divided into intense or moderate convective rainfall based on the scale of wavelet coefficients. These three precipitation types exhibit different microphysical features and raindrop-size distributions (Raut et al., 2020). For example, stratiform precipitation is characterized by small raindrops and the lowest raindrop density, while heavy convective precipitation has large drops and high droplet concentrations. Moderate convective rainfall is characterized by a high density of small and medium raindrop sizes, and a lack of large drops. To have a clear delineation between convective and stratiform rainfall, this study does not consider the moderate convective precipitation type.

TABLE 1 Attributes of two radars used in this study during summer (DJF) from 2011 to 2022.

Radar (ID)	Latitude	Longitude	Z–R relationship	Altitude	Fraction of missing data	Longest outage
Brisbane (66)	27.72° S	153.24° E	$Z = 283.4R^{1.32}$	174.9 m	1.81%	2 days
Townsville (73)	19.42° S	146.55° E	$Z = 355.5R^{1.19}$	612.5 m	0.41%	1 day

Quarterly Journal of the Royal Meteorological Society RMetS

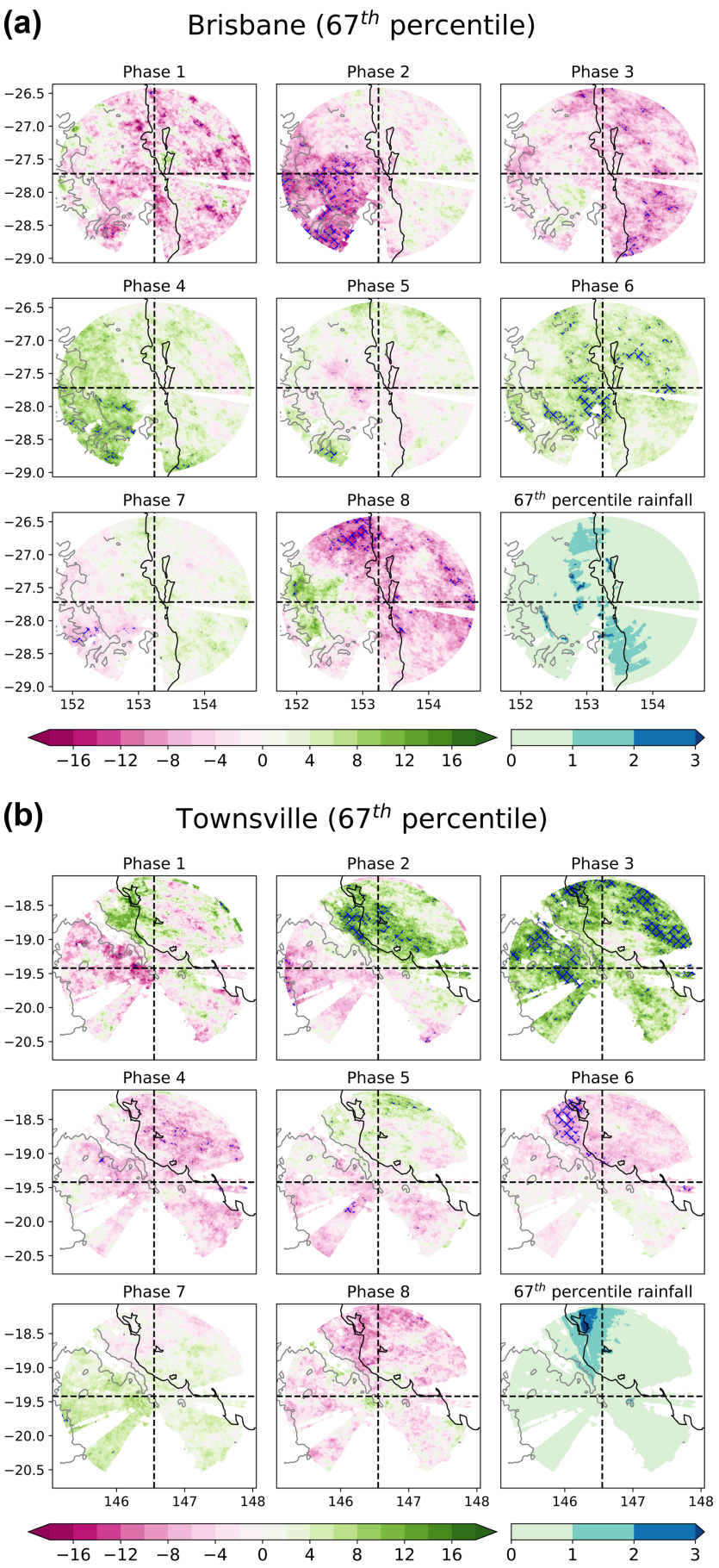

FIGURE 2 The first eight maps show the anomalies of daily rainfall probability exceeding the 67th percentile (%) during the austral summer (DJF) from 2011 to 2022 for different MJO phases at the (a) Brisbane radar and (b) Townsville radar. The 67th percentile rainfall threshold (mm · day^{-1}) is shown at the lower right corner of each set of radar plots. Areas with high beam blockage fraction are filtered out. Blue hatches indicate statistically significant rainfall results at the 90% level according to Monte Carlo testing. Grey contour lines show the altitude of orography above 500 m. [Colour figure can be viewed at wileyonlinelibrary.com]

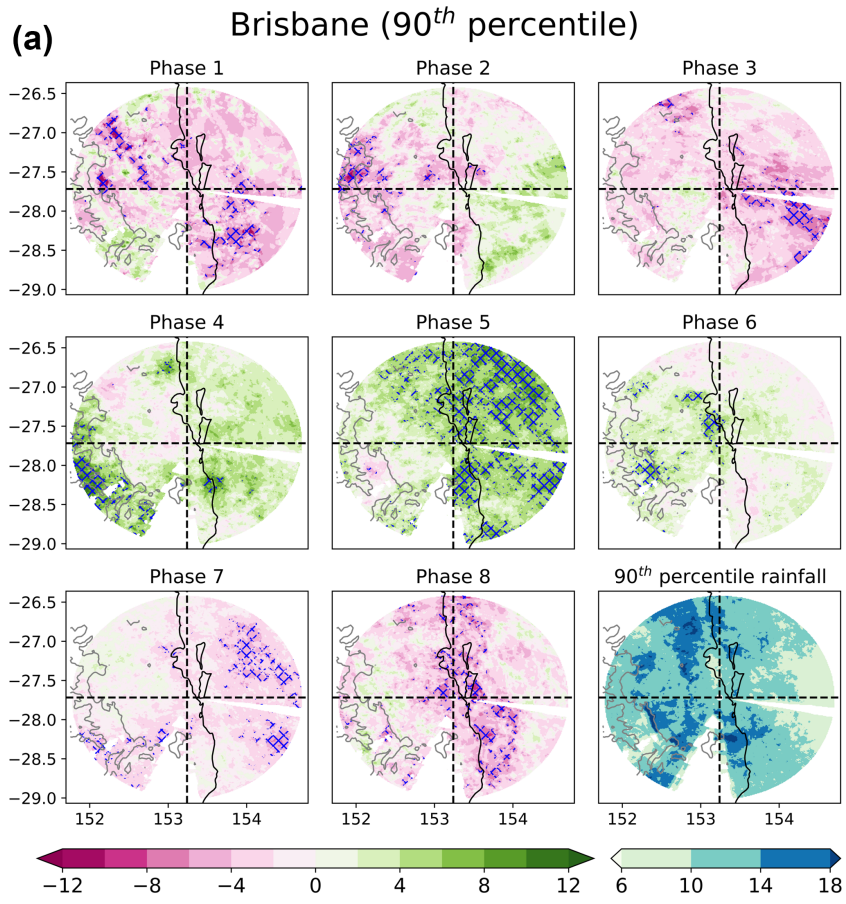

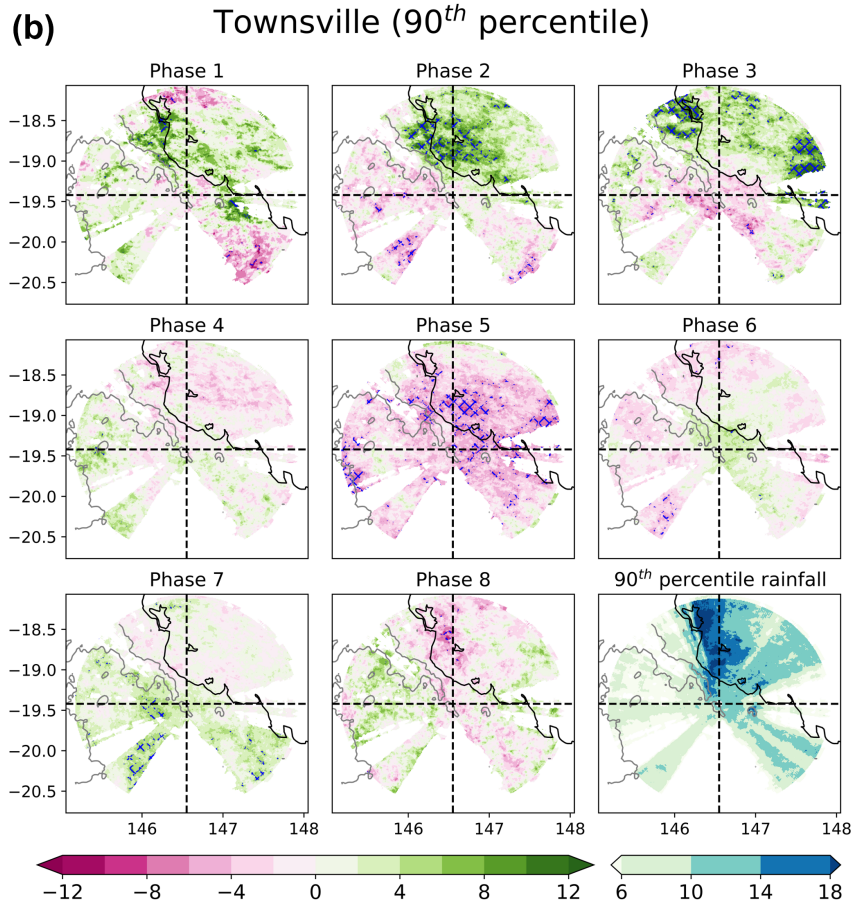

FIGURE 3 Same as in Figure 2, but for the 90th percentile of daily rainfall. [Colour figure can be viewed at wileyonlinelibrary.com]

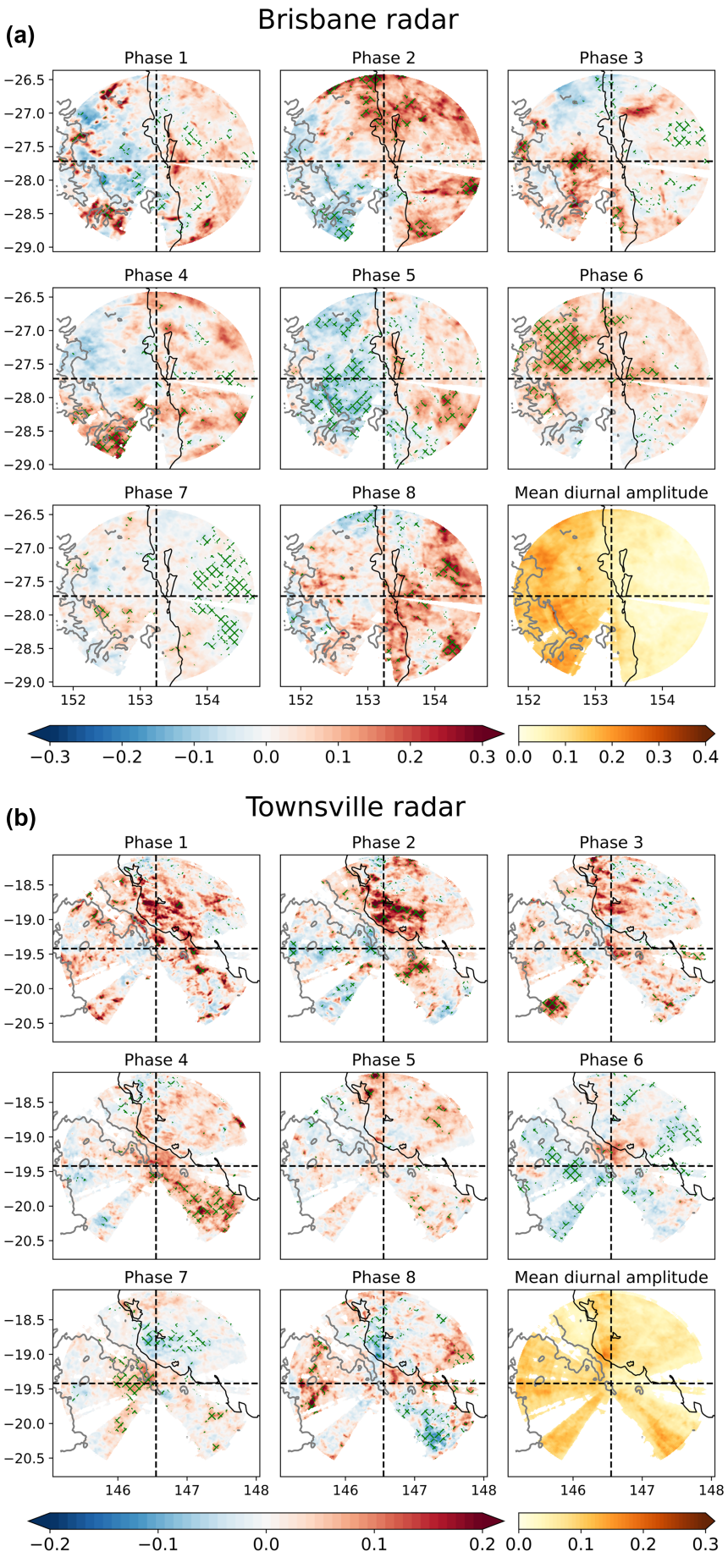

FIGURE 4 The first eight maps show the amplitude anomalies of the harmonic fit to the diurnal rainfall cycle during the summer (DJF) from 2011 to 2022 for different MJO phases at the (a) Brisbane radar and (b) Townsville radar. The average diurnal rainfall amplitude over the whole study period ($mm \cdot h^{-1}$) is shown at the lower right corner of each set of radar plots. Areas with high beam blockage fraction are filtered out. Green hatches indicate statistically significant rainfall results at the 90% level according to Monte Carlo testing. Grey contour lines show the altitude of orography above 500 m. Note that different colour scales are used for different radars (e.g., −0.2 to 0.2 for Townsville and −0.3 to 0.3 for Brisbane) to better represent the variation in diurnal rainfall amplitude with MJO at both radar locations. [Colour figure can be viewed at wileyonlinelibrary.com]

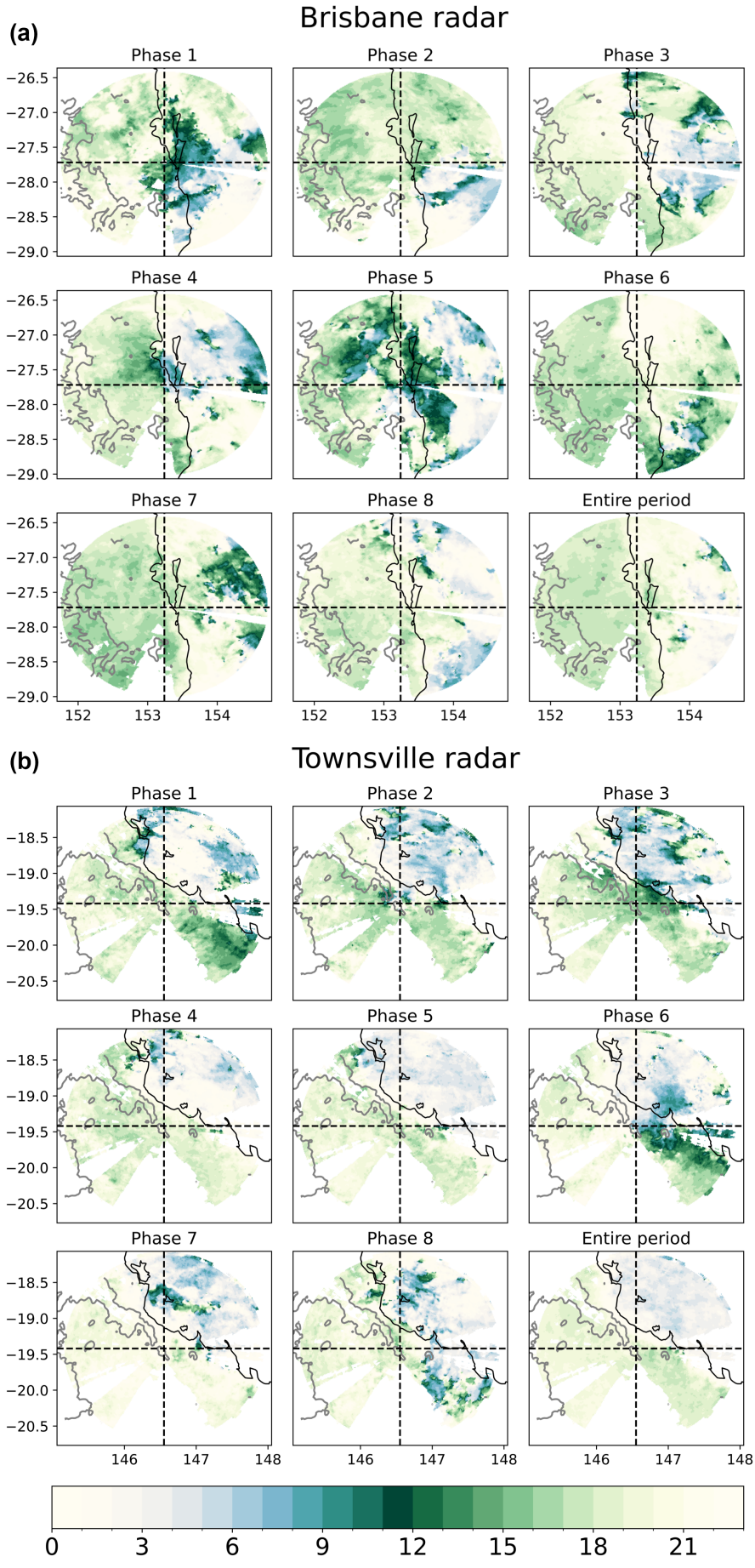

FIGURE 5 Timing of the peak of the fitted diurnal harmonic (local hours) during the summer (DJF) from 2011 to 2022 for the whole study period mean and different MJO phases at the (a) Brisbane radar and (b) Townsville radar. Areas with high beam blockage fraction are filtered out. Grey contour lines show the altitude of orography above 500 m. [Colour figure can be viewed at wileyonlinelibrary.com]

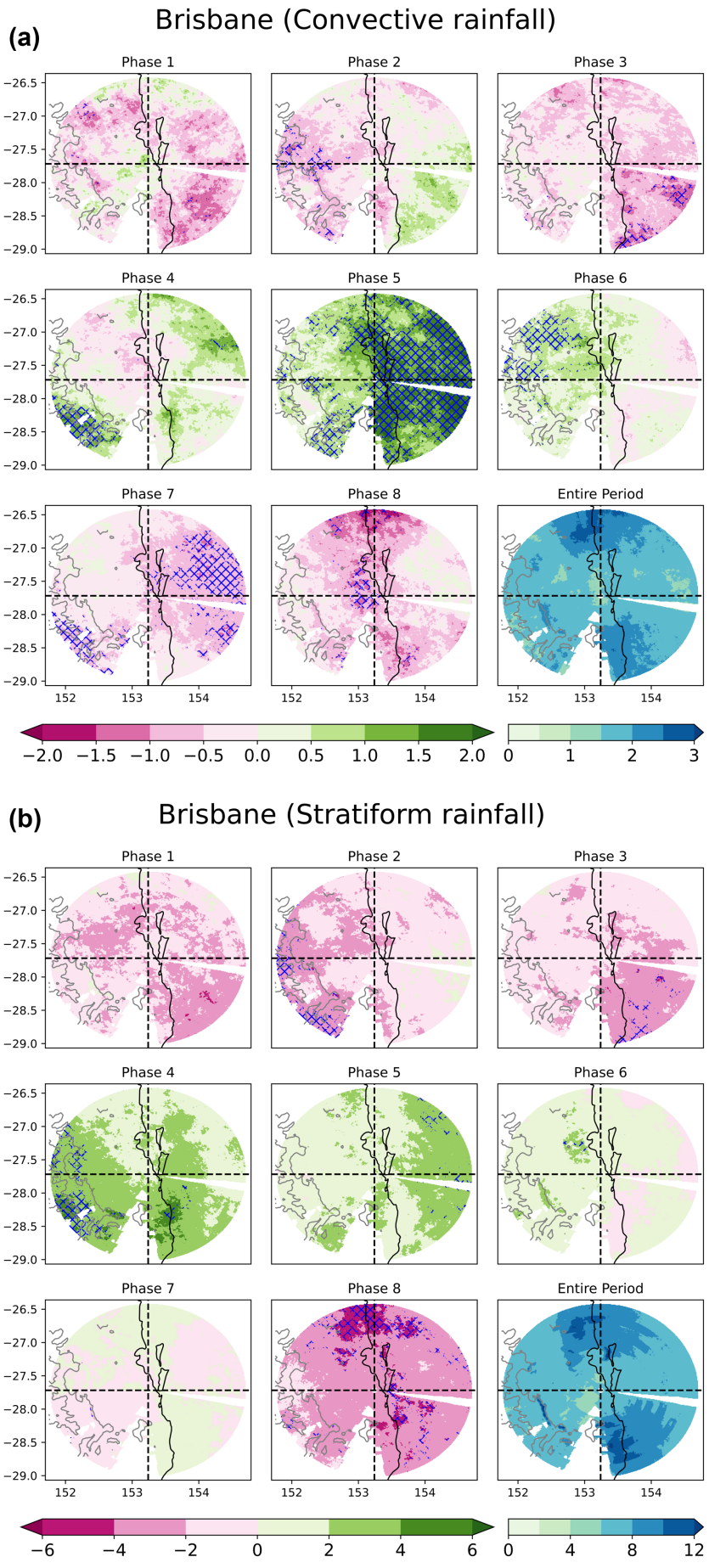

FIGURE 6 The first eight maps show the anomalies of the hourly frequency of convective rainfall (a) and stratiform rainfall (b) during the summer (DJF) from 2011 to 2022 for different MJO phases at Brisbane radar. The mean frequency of convective and stratiform rainfall over the whole study period (%) is shown at the lower right corner of panels (a) and (b), respectively. Areas with high beam blockage fraction are filtered out. Blue hatches indicate statistically significant rainfall results at the 90% level according to Monte Carlo testing. Grey contour lines show the altitude of orography above 500 m. Note that different colour scales are used for convective and stratiform rainfall. [Colour figure can be viewed at wileyonlinelibrary.com]

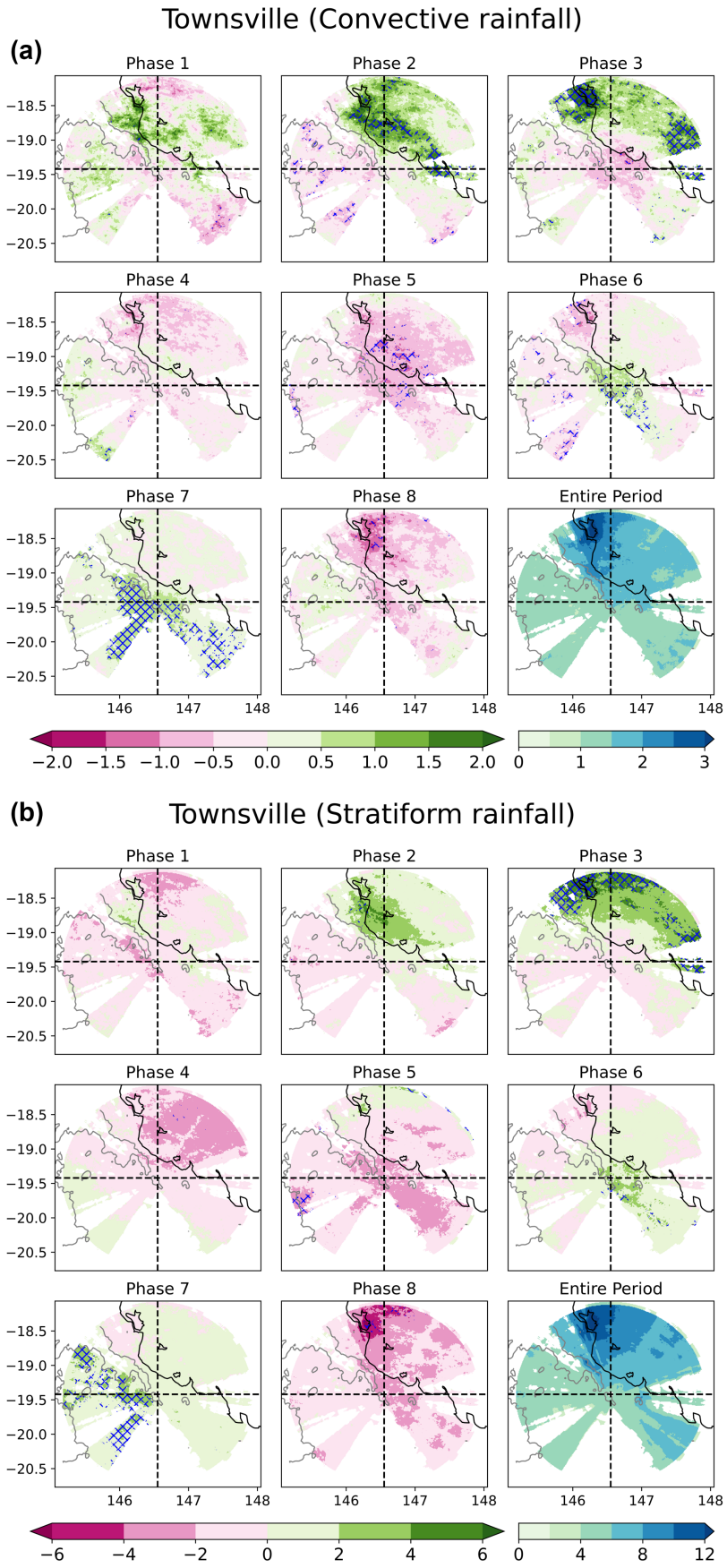

FIGURE 7 Same as in Figure 6, but for the Townsville radar. [Colour figure can be viewed at wileyonlinelibrary.com]

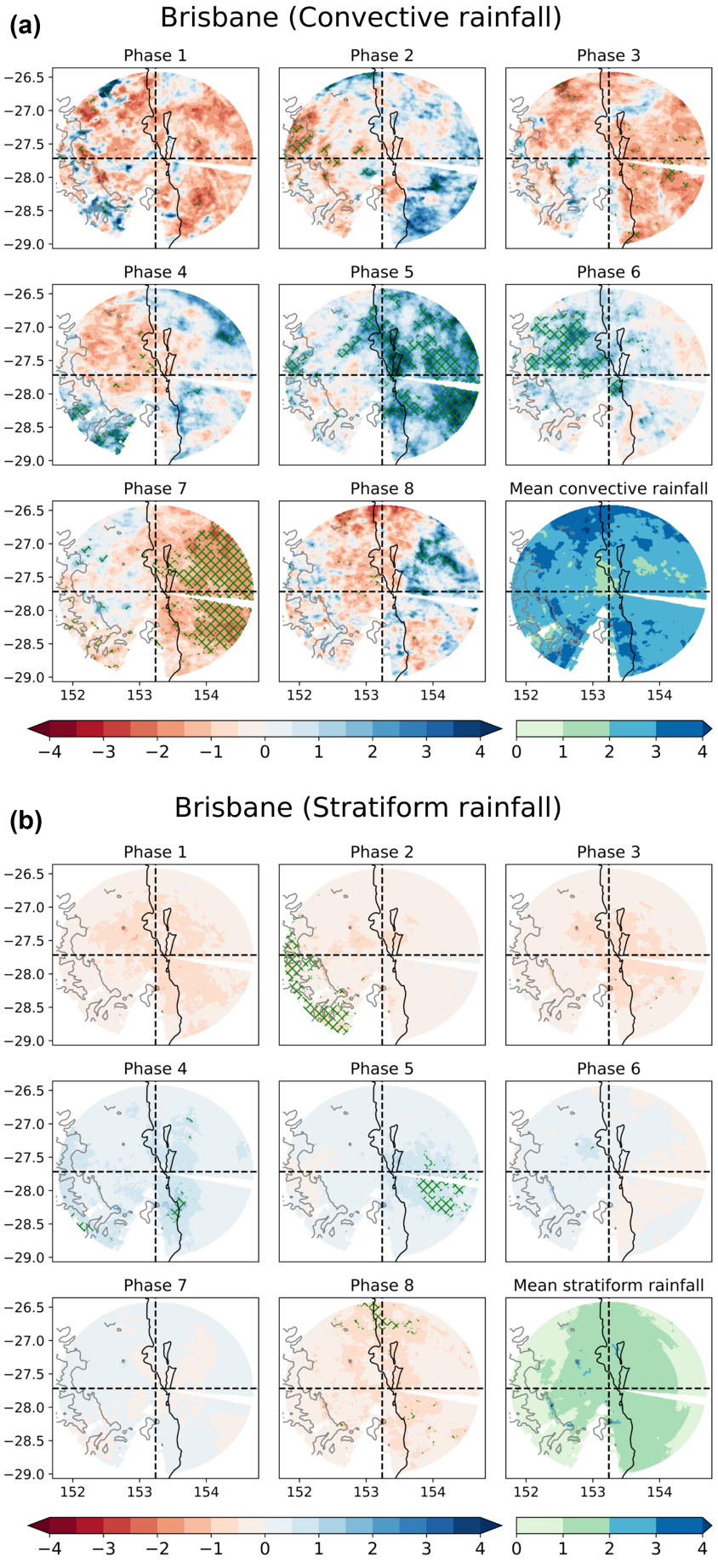

FIGURE 8 The first eight maps show the daily mean rainfall anomalies (mm · day^{-1}) for convective rainfall (a) and stratiform rainfall (b) during the summer (DJF) from 2011 to 2022 for different MJO phases at the Brisbane radar. The daily mean convective and stratiform rainfall over the whole study period (mm · day^{-1}) is shown at the lower right corner of panels (a) and (b), respectively. Areas with high beam blockage fraction are filtered out. Green hatches indicate statistically significant rainfall results at the 90% level according to Monte Carlo testing. Grey contour lines show the altitude of orography above 500 m. [Colour figure can be viewed at wileyonlinelibrary.com]

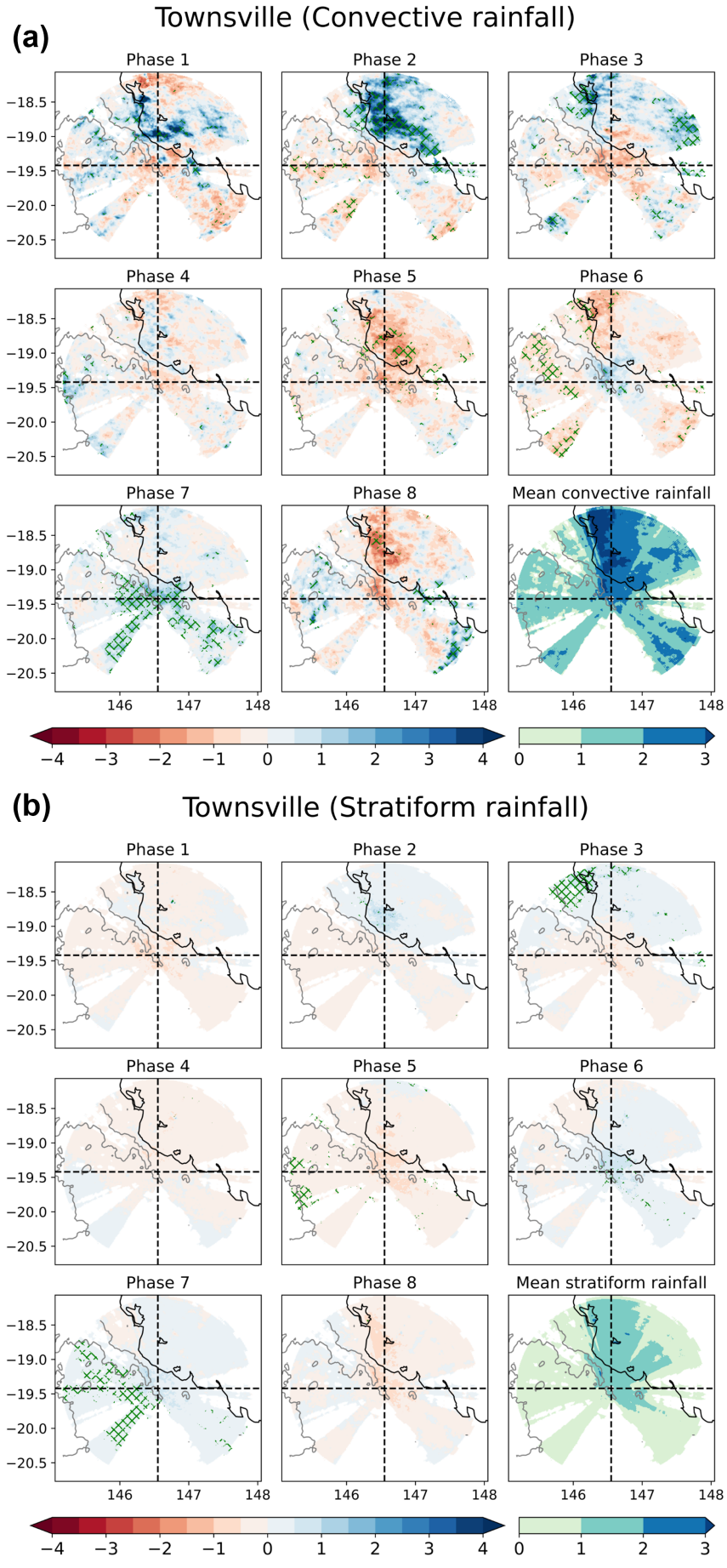

FIGURE 9 Same as in Figure 8, but for the Townsville radar. [Colour figure can be viewed at wileyonlinelibrary.com]

2.2 | Observational datasets

Observational datasets are utilized to investigate the change of large-scale and local-scale processes with MJO phases. Upper-air radiosonde sounding data obtained from the University of Wyoming data archive are used to examine the atmospheric vertical profiles during each MJO period. The analysis is based on 0000 UTC soundings (corresponding to 10 a.m. local time) and all sounding data are interpolated to standard pressure levels. Station 10-m wind data from the Australia Bureau of Meteorology are used to examine the change of mesoscale land–sea breeze with the MJO.

2.3 | Methods

This study uses the Real-time Multivariate MJO (RMM) index (Wheeler & Hendon, 2004) to classify the MJO phases. The index is calculated from a pair of multivariate empirical orthogonal functions (EOFs) of outgoing longwave radiation and zonal winds at 850 hPa and 200 hPa levels averaged over the equatorial region (15° S–15° N). The amplitude and phase of the MJO are then defined based on the first two principal components (PC1 and PC2). The entire cycle of the MJO is divided into eight phases based on the geographical location of the MJO tropical convection (Wheeler et al., 2009). Over NE Australia, phases 4–7 are often classified as enhanced convection phases, while phases 8, 1, 2, 3 are considered as suppressed convection phases of the MJO. We only select strong MJO events with amplitude of the RMM index greater than or equal to 1 for the analysis. During the 11-year study period, the number of days with strong MJO signals is 37 days for phase 1, 69 days for phase 2, 64 days for phase 3, 82 days for phase 4, 105 days for phase 5, 125 days for phase 6, 167 days for phase 7 and 61 days for phase 8.

For each radar grid point and for each MJO phase, the probability of daily rain rate exceeding a predefined rainfall percentile is calculated as the number of days with rain rate exceeding the threshold, divided by the total number of days in that MJO period. The rainfall probability anomalies for each MJO phase are then calculated by subtracting the climatological mean values over the whole study period. The 67th and 90th percentiles thresholds are used to understand the variation in daily mean and heavy precipitation with MJO phases, respectively. These percentile thresholds are commonly used to examine the modulation of precipitation with the MJO (Dao et al., 2023; Ghelani et al., 2017; Marshall et al., 2021; Wheeler et al., 2009) as they provide the flexibility with location and season. Dao et al. (2023) also found that the MJO-associated heavy precipitation patterns for the 90th and 95th percentiles are similar over NE Australia, therefore the 90th percentile is used in this study to obtain a greater number of events. The hourly frequency of convective/stratiform precipitation is calculated as the number of hours with convective/stratiform rainfall greater than $0.1\,\mathrm{mm}\cdot\mathrm{h}^{-1}$ divided by the total number of hours in each MJO period. A diurnal harmonic analysis is applied to understand the characteristics of diurnal precipitation cycle at two radar sites. This analysis provides information about the amplitude and timing of the diurnal rainfall peak. The diurnal harmonic cycle is idealized as a simple sine wave, with half of the 'peak-to-peak' amplitude shown in Figure 4 and the time of the positive peak indicated in Figure 5. Following similar methods in Vincent and Lane (2017), the diurnal harmonic is fitted to the average diurnal rainfall cycle (from 0:00 to 23:00 local time corresponding to the Queensland time zone) at each grid point, for the entire study period and for different MJO phases. Anomalies of atmospheric variables (e.g., wind, temperature, relative humidity) are calculated by subtracting the climatological mean of 11 DJF seasons.

Statistical significance for the precipitation features associated with MJO phases is evaluated using the Monte Carlo method, in which we simulate 1000 samples of the MJO phases vector by randomly shifting the MJO index (Dao et al., 2023; Rauniyar & Walsh, 2016; Wheeler et al., 2009). Note that a sample size of 1000 has been used in Monte Carlo methods in previous studies examining the impact of the MJO on rainfall (Dao et al., 2023; Muhammad et al., 2020; Pourasghar et al., 2019). For each shift, the precipitation results are recalculated for each MJO phase, and then the 5th and 95th percentiles values of the 1000 samples are chosen as the thresholds for significance at the 10% level for a two-tailed test. This test maintains the statistical features of the MJO (e.g., different number of days among MJO phases) and makes no assumptions about the normality of the data distribution. This method evaluates whether rainfall signals in each MJO phase are greater or smaller than what are expected from random weather variations. Note that with only 11 DJF seasons, some MJO phases (e.g., phases 1 and 8) have relatively small sample sizes. Therefore, the statistical significance test applied to the high-resolution radar data over a relatively short study period should be interpreted carefully considering the strong small-scale rainfall variability. The statistical significance is assessed independently at each grid point, and does not take spatially coherent signals into account. The results should be interpreted accordingly. Since the wind field is generally normally distributed, its statistical significance is assessed using Student's t test at a 90% confidence interval.

3 | THE VARIATION OF RADAR-DERIVED RAINFALL WITH MJO PHASES

3.1 | The variation of mean and heavy rainfall with MJO phases

Figure 2 shows the composite probability anomalies of rainfall exceeding the 67th percentile (hereafter Rf67) during eight MJO phases, as well as the 67th percentile rainfall values calculated from the entire study period for Brisbane and Townsville radar domains. In general, coastal and elevated topography areas receive a greater amount of precipitation (Figure S1), leading to higher percentile thresholds of rainfall compared to oceanic and inland areas. For example, the 67th percentile rainfall threshold over both radar domains is less than 1 mm · day^{-1} for most areas, except near the coast where values range from 1 to 2 mm · day^{-1} (bottom right subplot of Figure 2a,b). In addition, Townsville receives lower daily rainfall amounts (less than 3 mm · day^{-1}), except over the oceanic region, while Brisbane shows daily rainfall amounts ranging from 4 to 6 mm · day^{-1} across most of the radar domain (Figure S1). The rainfall probability anomaly maps for the Brisbane radar (Figure 2a) exhibit a large spatial variation during the eight MJO phases. Relative to the entire study period, the probability of rainfall exceeding the upper tercile threshold generally increases (positive Rf67) during phases 4–7 and decreases (negative Rf67) during phases 1–3 and 8 of the MJO. Statistically significant increases in rainfall frequency occur in phase 6, with an approximate 10% frequency increase compared to the mean probability over the entire period. This means that in phase 6, approximately 43% of the days have rainfall greater than the upper tercile threshold (33% as the probability of rainfall exceeding the 67th percentile threshold for the entire period, plus a 10% frequency increase). Significantly increased rainfall signals also appear in the southwestern part of the radar domain in phase 4. In contrast, rainfall probability decreases statistically significantly over the southwestern part of the radar domain in phase 2, and over the oceanic regions in phases 3 and 8. However, there are some notable exceptions to these general patterns. For example, over the high-terrain areas in the western part of the radar domain, rainfall probability is enhanced during phase 8 and decreased during phase 7 of the MJO.

At the Townsville radar (Figure 2b), the variation of rainfall likelihood with MJO phases reflects both large-scale and local influences. Rainfall probability generally increases (positive Rf67 values) during phase 7 and decreases (negative Rf67 values) during phases 4, 6, and 8 over the entire radar domain, and during phases 1, 2 and 5 over the land part. This is consistent with previous studies (Cowan et al., 2023; Dao et al., 2023; Wheeler et al., 2009) indicating that precipitation frequency in northern Australia increases during the enhanced convection phases, and decreases during the suppressed convection phases of the MJO. Using radar data, our results further show that a significantly enhanced precipitation signal is also observed over the oceanic portion of radar during phase 2 and over almost the entire radar domain during phase 3. The highest probability of precipitation exceeding the upper tercile values occurs in phase 3, with a frequency increase of approximately 16% compared to the climatological mean value. This is different from the conceptual model (Cowan et al., 2023; Wheeler et al., 2009) as in NE Australia, phases 2 and 3 are considered to be the suppressed convection periods of the MJO under which below-normal rainfall is expected. Using 64 years of rainfall data from the Australian Gridded Climate Data (AGCD), Dao et al. (2023) also showed increased daily rainfall probabilities during phase 3 of the MJO around Townsville. However, due to the coarse resolution of AGCD (approximately 5 km), it was not possible to examine the underlying processes or resolve the detailed spatial distribution of the rainfall. Positive Rf67 is also observed near the elevated topography areas and over the oceanic part of the radar domain during phases 1 and 5, but the signals are relatively weak.

To understand the influence of the MJO on heavy-rainfall events, we examined the anomalies of rainfall probability exceeding the 90th percentile threshold (hereafter Rf90) in each MJO phase (Figure 3). The 90th percentile rainfall maps show clear geographical variation with higher values observed near the coast and in elevated topography areas in both radars (bottom right subplot of Figure 3a,b). For the cBrisbane radar (Figure 3a), heavy-rainfall frequency increases during phases 4–6 (positive Rf90 values) and decreases during remaining phases of the MJO (negative Rf90 values). The most statistically significant enhancement of heavy-rainfall probability occurs over the ocean part of radar in phase 5 with a probability increase of about 10%. This means that the probability of receiving daily rainfall above the upper decile threshold over the ocean part of Brisbane radar is two times stronger in phase 5 (20%) compared to climatological mean condition (10% by definition). The enhanced heavy-rainfall signals also occur over the southwestern part of radar in phase 2. Some differences between the response of mean and heavy rainfall to the MJO at Brisbane radar are observed. For example, the probability of rainfall exceeding the 67th percentile threshold increases, but the rainfall probability exceeding the 90th percentile threshold decreases statistically significantly over the ocean part of radar during phase 7 of the MJO.

This indicates a shift in the distribution of rainfall in this phase towards more frequent light rain and less heavy rain. There is also a strong gradient of heavy-rainfall probability between the eastern and western portions of radar during phases 5 of the MJO, which is not obvious in the mean rainfall pattern. More heavy precipitation occurs in oceanic areas relative to the inland region in phase 5, and to a lesser extent in phase 2.

For the Townsville radar (Figure 3b), the heavy-rainfall probability increases significantly over the land part of radar domain during phase 7 with a probability of about 14%–16% (10% as the baseline probability of rainfall exceeding the 90th percentile threshold, plus a 4%–6% probability increase). The statistically significant increase in the heavy precipitation frequency also occurs over the oceanic part of the radar during phases 2–3 of the MJO, consistent with the mean rainfall pattern. Some discrepancies between the responses of mean and heavy precipitation to the MJO are also observed at the Townsville radar. For example, there is an increase in rainfall frequency (positive Rf67), but a significant decrease in the heavy-rainfall probability (negative Rf90) over the oceanic portion of the radar during phase 5. This difference will be discussed further in relation to the anomalous convective and stratiform rainfall (Sections 3.3 and 3.4). The spatial complexity of MJO-related rainfall is more obvious in heavy-rainfall patterns due to the smaller number of events.

The above results suggest that the MJO exhibits influences on both mean and heavy precipitation over coastal areas of NE Australia. The rainfall probability generally increases during the enhanced convection periods and decreases during the suppressed convection periods of the MJO, consistent with previous studies (Cowan et al., 2023; Dao et al., 2023; Marshall et al., 2021; Wheeler et al., 2009). However, there are some notable exceptions to this general notion in both radar domains. During the suppressed convection phases when rainfall is expected to be below normal, some locations show increased precipitation probabilities. For example, at the Townsville radar, rainfall frequency increases statistically significantly during phase 3, which is one of the suppressed convection phases of the MJO. Our results also indicate some differences in the responses of mean and heavy precipitation to the MJO, which were not reported in previous studies. These results suggest that there is a multiscale interaction between local features (e.g., topography, land–sea breezes) and large-scale forcings in regulating both the frequency and intensity of rainfall over coastal areas of NE Australia. Details of the possible mechanisms controlling the local precipitation response to the MJO will be discussed in Section 4.

3.2 | Influence of the MJO on the diurnal cycle of radar-derived rainfall

In addition to daily mean and heavy-rainfall patterns, the diurnal cycle of rainfall is also modulated by the MJO over many regions (Dao et al., 2023; Peatman et al., 2014; Rauniyar & Walsh, 2011; Vincent & Lane, 2016). In this section, we examine how the MJO affects the diurnal rainfall variation over the coastal areas of NE Australia.

Figure 4 shows the peak amplitude of the diurnal rainfall harmonic for the whole-study period and its anomalies for eight MJO phases. At the Brisbane radar (Figure 4a), there is a strong gradient in the diurnal peak amplitude of precipitation between the ocean and land areas, with higher values (about 0.3 $mm \cdot h^{-1}$) occurring over the land. The rainfall diurnal harmonic amplitude accounts for approximately 15% of the mean rainfall over land, compared to about 4% over the ocean, suggesting that diurnal forcings have a stronger impact over land than the ocean part of the Brisbane radar. The maximum peak amplitudes of diurnal rainfall variation are observed near regions with high orography (above 500 m). Similar to the daily rainfall pattern (Figures 2a and 3a), the diurnal rainfall amplitude anomalies also show a clear west–east gradient in most MJO phases. It is interesting to note that the increased and decreased diurnal rainfall amplitude at the Brisbane radar do not closely align with the suppressed and enhanced convection MJO phases. Compared to the mean diurnal amplitude over the whole study period, the diurnal peak of ocean-based precipitation generally decreases (negative anomalies) during phase 7 and increases (positive anomalies) during the remaining MJO phases. The spatial complexity of diurnal rainfall amplitude anomalies during eight MJO phases is more obvious over the land part of the radar domain. The diurnal peak of land-based rainfall decreases statistically significantly in phase 5 and increases statistically significantly in phase 6 of the MJO. These results are not consistent with studies from the deep tropics that have found a suppressed diurnal cycle during the MJO active phase and an enhanced diurnal cycle in the preceding phases (e.g., Peatman et al., 2014; Vincent et al., 2016).

The land–sea contrast in mean diurnal amplitude over the whole study period, as well as in diurnal amplitude anomalies during eight MJO phases is less pronounced at the Townsville radar (Figure 4b). Over the ocean part, the diurnal peak amplitudes are typically weaker during phases 6 and 7, and stronger during phases 1–5 of the MJO. The peak amplitude of diurnal rainfall variation over the land part also decreases statistically significantly during phase 6 of the MJO. The weaker and stronger diurnal amplitudes generally align with the enhanced and

suppressed convection phases of the MJO, respectively, consistent with other studies from the Maritime Continent (Love et al., 2011; Peatman et al., 2014; Rauniyar & Walsh, 2011; Vincent et al., 2016; Wei et al., 2020). Greater spatial nuances in the diurnal precipitation amplitude are observed during the suppressed convection phases of the MJO. For example, the diurnal amplitude of rainfall increases significantly over the ocean part, but decreases significantly over land part of radar domain during phase 2, consistent with the observed rainfall pattern in this phase (see Figures 2b, 3b and 4b for comparison).

The spatial distribution of the timing of maximum diurnal rainfall at the two radars is illustrated in Figure 5. An offshore propagation of precipitation peak is observed at the Brisbane radar (Figure 5a). For the whole study period, maximum precipitation occurs in the late afternoon over land, at night along the oceanic coast, and in the early morning over the ocean. This different timing could be associated with the diurnal cycle of solar radiative heating at the surface and local circulations such as land–sea circulation. A late afternoon/evening rainfall peak dominates over the land part in all MJO phases, although there are spatial and temporal variations among eight MJO phases. For example, maximum rainfall over land occurs later during some suppressed convection phases of the MJO (e.g., phases 8, 1 and 3). The timing of the peak rainfall over the ocean varies with MJO periods. An early morning rainfall peak is observed over most oceanic regions during phases 5 and 8, as well as in some oceanic regions during phases 1–4. Notably, phase 5 shows the most obvious contrast in rainfall peak timing between the ocean and land part of the radar domain, with a morning peak over the sea and an afternoon peak over the land, consistent with this phase exhibiting the strongest east–west gradient in rainfall pattern (see Figures 3a and 5a for comparison). By contrast, a late afternoon/evening precipitation peak occurs over most oceanic regions during phases 6 and 7 of the MJO, suggesting that the land–sea breeze circulation might not be the sole factor driving the diurnal cycle of rainfall during these phases. Previous studies show that the background wind has influences on the rainfall diurnal cycle and associated land–sea breezes circulation over the tropics (Bui et al., 2023; Natoli & Maloney, 2023a; Natoli & Maloney, 2023b; Short et al., 2019) and that the background wind seems to have an impact on the timing differences of the diurnal rainfall maximum among MJO phases (Lestari et al., 2022; Oh et al., 2012).

Around the Townsville radar (Figure 5b), the land–sea difference in the timing of the rainfall peak is obvious for the entire period as well as for all MJO phases. This differs from the results of the Brisbane radar, suggesting that the characteristics of the diurnal cycle of MJO-related precipitation vary by location. Over the ocean, maximum diurnal precipitation occurs during the night/early morning for all MJO phases; however, there are still time differences among MJO phases. For example, phases 2 and 3 tend to have a later morning rainfall peak over the ocean compared to other MJO phases. Note that significantly increased rainfall probabilities are observed over the oceanic part of the radar domain during these phases (see Figures 2b and 3b). The spatial pattern of the diurnal peak time over the land part of the Townsville radar exhibits geographical variations. For the whole study period, a late afternoon/evening maximum precipitation is found over most land regions, except for the southern coast where rainfall peaks earlier. This feature is also evident in some MJO phases (e.g., phases 1, 6 and 8). During the enhanced convection phases (e.g., phases 6 and 7) maximum diurnal precipitation over land occurs later (late evening/midnight) compared to the suppressed convection phases of the MJO (e.g, phases 1–5 and 8).

These above results indicate that the MJO has influence on the diurnal cycle of precipitation over coastal areas of NE Australia. Rainfall reaches its maximum in the afternoon over land and in the morning over the ocean part of the radar coverage under most MJO phases. The amplitude of diurnal precipitation variability in suppressed convection phases is generally larger than in enhanced convection phases of the MJO. These findings are consistent with previous studies (Dao et al., 2023; Peatman et al., 2014; Rauniyar & Walsh, 2011; Vincent & Lane, 2016). Using radar data and considering each MJO phase separately, this study further shows that the diurnal precipitation variation associated with the MJO is spatially inhomogeneous and is likely regulated by local forcings. These local-scale variations may not be evident in studies based on coarser resolution information from satellite or gridded based station data. The impact of the MJO on diurnal rainfall characteristics (e.g., diurnal timing and amplitude) varies from phase to phase. Thus, it is necessary to examine rainfall variability in each individual MJO phase as each period may be associated with different influences of local forcings. Similar to the daily rainfall variation with MJO phases (Section 3.1), the changes of rainfall diurnal features with the MJO over coastal areas of NE Australia also reflect the interplay between local processes (e.g, land–sea breeze circulation) and large-scale background processes, which will be discussed in more detail in Section 4.

3.3 | The variation of radar-derived convective and stratiform rainfall frequency with MJO phases

This section examines the modulation of the MJO on convective and stratiform rainfall to understand how rainfall

characteristics change with different MJO regimes. The frequency of hourly convective and stratiform precipitation over the whole study period as well as its anomalies during eight MJO phases at the Brisbane radar location are illustrated in Figure 6. The spatial distribution of convective rainfall frequency anomalies is relatively similar to that of heavy-rainfall frequency anomalies (see Figures 3a and 6a for comparison), suggesting strong convective contribution to in heavy-rainfall events. Increased convective rainfall signals (positive anomalies) are observed in some locations of the radar during phases 1 and 2, becoming more widespread during phases 4–6 of the MJO. The occurrence likelihood of convective rainfall at the Brisbane radar increases statistically significantly during phase 5, and decreases statistically significantly during phase 7 of the MJO over the ocean part of radar. The highest increase in hourly convective rainfall frequency is observed during phase 5, with the rainfall frequency reaching approximately 4% over the ocean part of the radar (2% as the convective rainfall frequency in the study period mean, plus a 2% frequency increase). This means that, compared to the climatological mean condition, the probability of having convective precipitation is about two times higher during this phase. There is also an obvious difference in convective precipitation frequency between the land and oceanic part of the radar domain in phases 2, 5 and 6 of the MJO, consistent with the rainfall pattern (see Figure 3a). Stratiform rainfall is found to be the most common rainfall type at Brisbane with a frequency of about 8% in the study period mean (Figure 6b). The variation of stratiform rainfall frequency with the MJO is slightly different from that of convective rainfall. Stratiform rainfall frequency increases during phases 4–7 and decreases during phases 8, 1–3 of the MJO, consistent with the enhanced and suppressed phases of the MJO (Figure 6b). The spatial distribution of the MJO-associated stratiform rainfall is more uniform across the entire radar domain as stratiform often occurs over broader area (Houze Jr. et al., 2015; Houze Jr., 1997; Powell & Houze Jr., 2013) and is less subject to orographic enhancement.

Over Townsville, higher frequencies of both convective and stratiform precipitation are observed over the oceanic part compared to the land part of the radar domain (Figure 7). The frequency of convective rainfall increases (positive anomalies) predominantly over the ocean part during phases 1–3 and over the land part during phase 7, albeit with a smaller amplitude (Figure 7a). A decrease in convective rainfall frequency is observed in most areas during the remaining MJO phases (e.g., phases 4–6, 8). The most significant increase in convective precipitation frequency is observed over the oceanic region during phases 2 and 3, with an occurrence probability of approximately 3.5%–4% (2% as the hourly convective rainfall frequency in the study period mean, plus a 1.5%–2% frequency increase). This indicates that, compared to the entire study period mean, the probability of experiencing convective precipitation over the oceanic part of the Townsville radar increases by 1.5–2 times during these phases. Similar to the Brisbane radar, stratiform rainfall is also the most common type at the Townsville radar, with a frequency of about 4%–6% over the land region, and approximately 8% over the oceanic region for the study period mean. There are also differences between the variation in convective and stratiform rainfall frequency with MJO phases at the Townsville site. For example, an increase in stratiform rainfall frequency is observed in phases 2 and 3 over the oceanic part and in phases 6 and 7 over almost the entire radar domain. The most notable difference is observed in phase 1, where the anomalous frequency has different signs, although we note that this is the phase with the least days, which limits the significance of this result. The spatial distribution of convective and stratiform rainfall frequencies at Townsville is much more similar than at the Brisbane radar (see Figures 6 and 7 for comparison).

3.4 | The variation of radar-derived convective and stratiform rainfall amount with MJO phases

To understand the relative contribution of convective and stratiform precipitation to the variation of the total daily precipitation amount with the MJO, we further examined the convective and stratiform rainfall anomalies during different MJO phases at two radar sites. Figure 8 shows the variation of stratiform and convective rainfall intensity with MJO phases at the Brisbane radar. Although stratiform rainfall occurs more frequently, convective rainfall contributes predominantly to the total rainfall (approximately 2–3 $mm \cdot day^{-1}$ over the study period mean, Figure 8a). Similar to the convective rainfall frequency map, the highest increase in convective rainfall amount is observed during phase 5 of the MJO over the oceanic part of the radar domain, with the rainfall anomaly reaching about 4 $mm \cdot day^{-1}$. Enhanced convective rainfall signals are also found in certain areas of the radar during the suppressed convective phases of the MJO (e.g., phases 1, 2 and 8). In contrast, increased stratiform rainfall is only observed during the enhanced convection phases of the MJO (phases 4–7, Figure 8b). This aligns with previous findings over the deep tropics, which used TRMM precipitation radar (Alber et al., 2023; Bai, 2021; Vincent & Lane, 2018) and C-band Doppler radar (Lestari et al., 2022) to indicate that stratiform rainfall increases with the onset of the MJO enhanced convection. The influence of the MJO on convective rainfall is stronger

and more statistically significant than that of stratiform rainfall at the Brisbane radar. Importantly, the anomalous frequency (Figure 6a) and anomalous rainfall contribution (Figure 8a) of convective rainfall do not always have the same sign. For example, the statistically significant increase in rainfall contribution in phase 8 over the ocean is accompanied by no change or a slight decrease (not significant) in rainfall frequency, indicating that the convective rainfall might be heavier. Conversely, some statistically significant increases in rainfall frequency in phase 5 over the land are associated with almost no change or a slight decrease in rainfall contribution (not significant), suggesting that the convective rainfall may not be very intense. These results together indicate a change in the distribution of rainfall intensity.

Convective precipitation dominates the total rainfall at the Townsville radar, with daily mean amounts of 2–3 $mm \cdot day^{-1}$ over the oceanic region, and 1–2 $mm \cdot day^{-1}$ over the land region of the radar domain. Increased convective rainfall is mostly observed over the ocean during phases 1–3, and over land during phase 7 of the MJO (Figure 9a). The most significant increase in convective rainfall occurs along the seaward side of the coast during phase 2, with an increase of approximately 3 $mm \cdot day^{-1}$ compared to the average convective rainfall over the whole study period. The variation of stratiform rainfall with the MJO is comparatively weaker than that of convective rainfall. Positive rainfall anomalies occur over most of the radar domain during phase 7 (Figure 9b), consistent with the increased stratiform frequency observed in this phase (Figure 7b). Interestingly, enhanced stratiform precipitation signals are also observed over the oceanic region during phases 2–3, albeit with much weaker amplitude and not statistically significant compared to convective precipitation. Note that Townsville lies between the tropical and subtropical zones, so its precipitation can be modulated by both direct and indirect influences of the MJO.

The above results suggest that the MJO has influence on both frequency and intensity of convective and stratiform rainfall over the coastal areas of NE Australia. Although stratiform rainfall occurs more frequently, convective rainfall is the dominant contributor to total rainfall at the two radar locations. The influence of the MJO on convective rainfall tends to be stronger and more statistically significant than that of stratiform rainfall over the coastal areas of NE Australia. The widespread enhanced rainfall probability during the enhanced convection phase of the MJO is likely due to increases in both stratiform and convective rainfall. This is different from previous findings over the deep tropics where an increased likelihood of light rain rate but a reduced likelihood of heavier rain rate was observed during the active MJO phases (Lestari et al., 2022). The findings of Lestari et al. (2022) were consistent with those of Vincent and Lane (2018), who partitioned the diabatic heating budget of Sumatra into convective and stratiform types and showed that the diabatic heating from convective processes peaked one to two MJO phases ahead of the diabatic heating from stratiform processes in convection-permitting simulations. Our results, at higher latitudes, only partly reflect the conclusions of Lestari et al. (2022) and Vincent and Lane (2018), with an increase in convective precipitation preceding an increase in stratiform precipitation by 1–2 phases. This likely indicates the influence of other processes modulating the rainfall response to the MJO outside of the deep tropics. The locally increased rainfall probability during some suppressed convection phases of the MJO at both radars mainly comes from the increase of convective rainfall, consistent with previous studies over Maritime Continent showing that convective rainfall increases during inactive MJO phases due to enhanced clear-sky insolation (Bai, 2021; Vincent & Lane, 2018).

4 | POSSIBLE SCALE INTERACTION MECHANISMS REGULATING THE MJO-RELATED LOCAL RAINFALL PATTERNS

4.1 | The variation of environmental variables with MJO phases

The inhomogeneous local rainfall patterns associated with the MJO suggest interactions between the background thermodynamics, which encapsulate the coastal and topographic forcings, as well as moisture transport. Here we examine how these factors may interact with the background winds using daily 0000 UTC (10 a.m. local time) radiosonde soundings from Brisbane and Townsville airports. Figure 10 shows the anomalies of temperature, U and V wind components and relative humidity (RH) at the two sites for each MJO phase. For the Brisbane radar, the enhanced rainfall signal during phases 5 and 6 is associated with the anomalous low-level northerly winds, while the suppressed precipitation during phases 1–3 and 8 occurs in the presence of southerly anomalies. These wind anomalies are associated with the large-scale circulation of the MJO, with enhanced convection signals occurring during phases 5 and 6 and suppressed convection signals during phases 8 and 1–3 over Australia (Figure S2). This is consistent with Wheeler et al. (2009) indicating that in extratropical Australia, increased rainfall probability with the MJO results from anomalous northerlies transporting moisture from the tropics, and decreased rainfall is associated with southerly wind anomalies. The

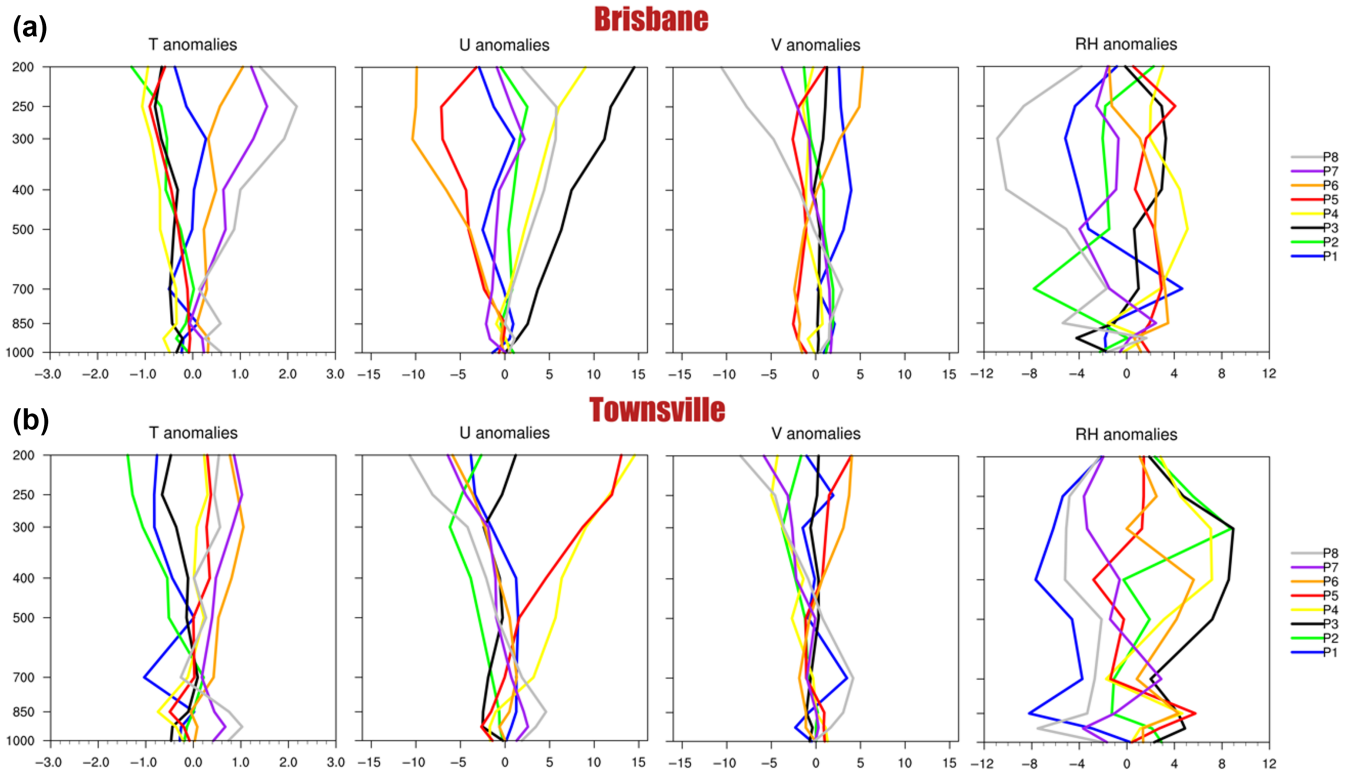

FIGURE 10 The vertical profile of temperature (units: K), horizontal wind (units: $m \cdot s^{-1}$) and relative humidity (units: %) anomalies during austral summer (DJF) from 2011 to 2022 for different MJO phases at (a) Brisbane station and (b) Townsville station. Anomalies are relative to the seasonal mean. [Colour figure can be viewed at wileyonlinelibrary.com]

TABLE 2 The convective available potential energy (CAPE) and convective inhibition (CIN) values for the most unstable parcel (units: $J \cdot kg^{-1}$) averaged for different MJO phases.

		1	2	3	4	5	6	7	8	Mean
Brisbane	CAPE	196.3	270.4	289.2	168.9	330.1	308.8	268.6	210.9	255.4
	CIN	−57.9	−30.4	−33.2	−50.8	−32.9	−28.3	−31.1	−26.6	−36.4
Townsville	CAPE	530.1	593.6	372.4	338.5	443.5	414.3	499.9	539.6	466.5
	CIN	−24.4	−34.4	−18.5	−24.8	−24.3	−35.3	−41.9	−48.9	−31.6

result is also consistent with other previous studies examining the variation of mean and extreme precipitation with the MJO in Australia (Cowan et al., 2023; Dao et al., 2023; Marshall et al., 2021). Our results further indicate that rainfall under the different MJO phases is likely comodulated by multiple factors. For example, at Brisbane, there appears to be strong positive relative humidity anomalies in phases 4, 5 and 6, consistent with the 'moist' nature of these MJO phases. However, there are other factors regulating the amount and type of precipitation. Phase 4 shows weak negative temperature anomalies increasing with height and also weak wind anomalies in both U and V components. In addition, a lower convective available potential energy (CAPE) and higher convective inhibition (CIN) value is observed in phase 4 compared to phases 5 and 6 (Table 2). These features are expected to reduce the capacity for instability, moisture transport and convergence. Phase 5, on the other hand, shows deep and strong easterly and northerly anomalies which enhances moisture transport, increased negative temperature anomalies with height, and the highest CAPE value among the eight MJO phases, consistent with the fact that this is the rainiest phase. Phase 6 shows deep easterly and northerly wind anomalies and positive relative humidity anomalies, but increased positive temperature anomalies with height, indicating more stable conditions than phase 5 (similar CIN values but the CAPE value in phase 6 is smaller than in phase 5). Similarly, phases 2 and 8 are

the two dry phases, where both show southerly anomalies, but phase 2 shows increased negative temperature anomalies with height in contrast to increased positive temperature anomalies with height in phase 8. In addition, the CAPE value in phase 2 is larger than in phase 8, consistent with the fact that phase 2 has more frequent rain than phase 8. A similar analysis can be conducted for Townsville, where we see that the phases with deep positive moisture anomalies are 3, 4, and 6, but only phase 3 shows widespread rainfall, consistent with this having the strongest deep easterly flow propagating onshore, which may interact with the topography inducing convection, and the smallest CIN value. This is in contrast to the larger-scale MJO rainfall variability over NE Australia (Dao et al., 2023), which does show enhanced rainfall probabilities under the MJO active phases of 5–7, and demonstrates that locally, the background wind may modulate the larger-scale rainfall patterns. The deep easterly anomalies (up to 500 hPa) observed in phase 3 are likely not solely due to shallow trade winds but also represent the influences of other large-scale features. For example, strong anomalous easterlies are also evident in the MJO-associated large-scale circulation during this phase over northern Australia (Figure S2). The above results highlight that it is critical to understand the relative importance of the different factors under the different phases of MJO.

4.2 | The variation of land–sea breezes with MJO phases

One important aspect of the local-scale modulation of the MJO variability is the variation in strength and extent of the land–sea breeze circulation. In the deep tropics, the MJO affects the diurnal rainfall cycle and its associated land–sea breezes through regulating background winds (Natoli & Maloney, 2023b; Short et al., 2019), moisture availability (Bretherton et al., 2004; Vincent & Lane, 2017) and solar radiation received at the surface (Birch et al., 2016; Peatman et al., 2014; Rauniyar & Walsh, 2011). In this work we used weather station data at high temporal resolution (half hourly) to examine the variation of land–sea breeze strength during different MJO periods in the two radar domains. Land–sea breeze is a local circulation driven by the thermal contrast between land and sea, which has been shown to have influences of both a near-shore density current and a diurnally forced gravity wave propagating upwards and outwards from the coast (Bai, 2021; Love et al., 2011; Miller et al., 2003; Peatman et al., 2023). Given the proximity to the coastline, we assume that the land–sea breeze perturbations are mostly related to a density current.

Isolating the land/sea breezes from observations is challenging as the observed winds are often influenced/masked by other local factors (e.g., downslope/upslope winds over coastal mountains). However, the availability of multistation wind data along the coast is helpful in characterizing the spatial wind patterns that are pertinent to land–sea breezes. Assuming that large-scale winds have relatively weak diurnal variation, the local land–sea breezes (wind anomalies) are estimated by subtracting daily mean winds from the total winds at each hour, following previous studies (Chen et al., 2016; Huang et al., 2015; Li et al., 2021; Shen et al., 2019; Vincent & Lane, 2017). A perturbation wind with a direction between 0° and 180° (assuming a north–south orientated coastline) is classified as offshore (land breeze), while a direction between 180° and 360° indicates onshore (sea breeze). From the average diurnal cycle of wind perturbation in each MJO phase, the maximum seaward and landward wind perturbations are selected to represent the land and sea breezes, respectively (Figure 11). To provide a more quantitative understanding of how the land–sea breeze changes with MJO phases, the amplitude of the land–sea breeze circulation is estimated by calculating the difference between the maximum seaward and landward wind perturbations. To ensure alignment, only the wind component perpendicular to the coast is considered in this calculation. To calculate the perpendicular wind component, we first divide the coastline into straight line-segments and then determine the perpendicular wind component relative to the nearest coastline segment for each station. It is worth noting that the estimated land/sea breezes derived in this study are consistent with the timing of land/sea breezes expected over eastern Australia (Soderholm et al., 2016, 2017) and show a distinct diurnal wind reversal, suggesting that these estimates are representative of the general land/sea breeze patterns in this region, despite the influence of other local factors.

For the Brisbane radar (Figure 11a), the stronger (positive anomalies) and weaker (negative anomalies) land–sea breeze circulation are inconsistent with the suppressed and enhanced convection phases of the MJO. For example, the most weakened and enhanced land–sea breeze circulation are both observed during the suppressed convection phase of the MJO (phases 1 and 3). This again emphasizes the importance of examining local rainfall variations in each MJO phase separately in extratropical regions, as each phase may have different local influences. Land–sea breezes significantly weaken during phase 1 and strengthen during phase 3 of the MJO, generally consistent with the decreased and increased diurnal rainfall amplitude over land part of the radar domain during these phases (see Figures 4a and 11a for comparison). These are the

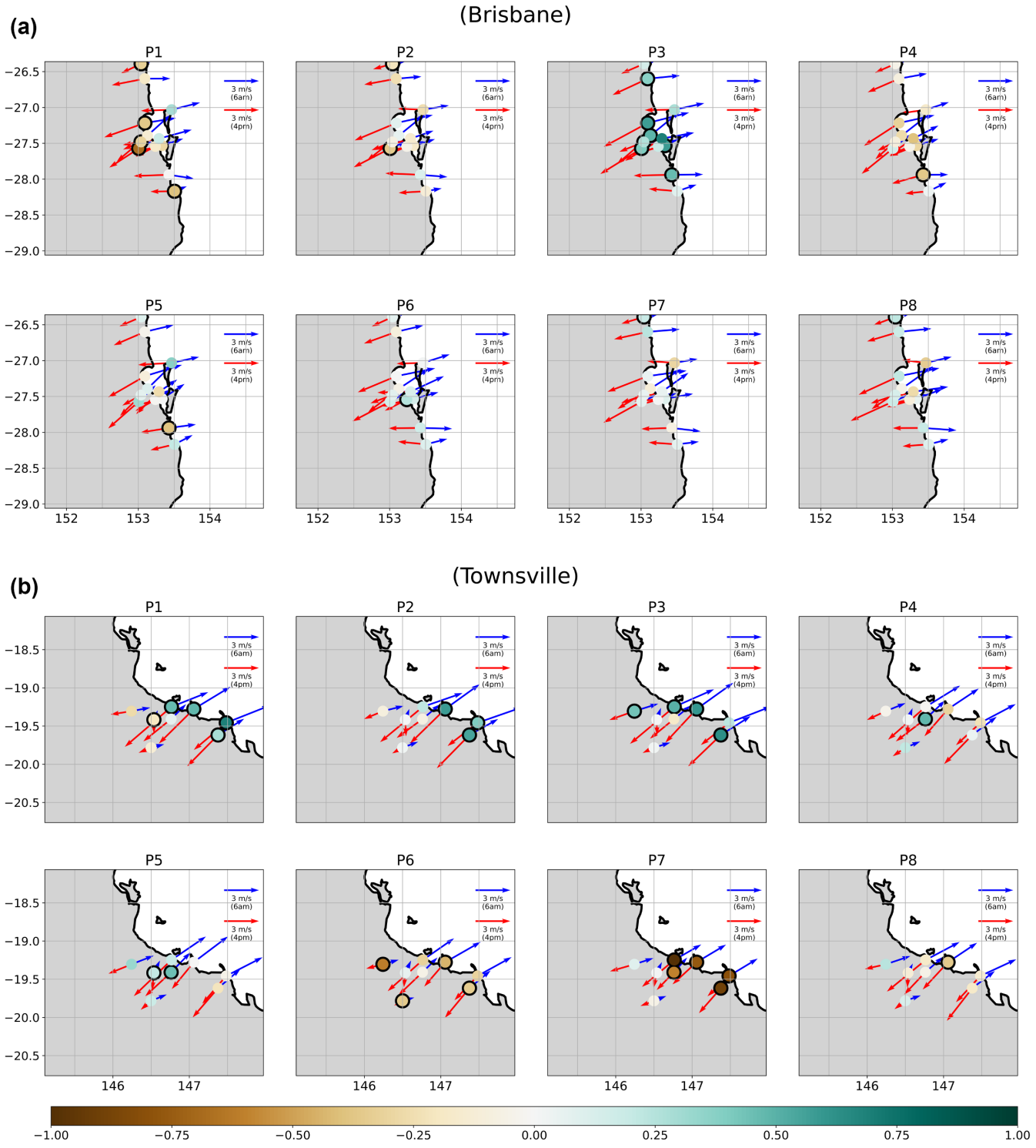

FIGURE 11 The composite of land–sea breeze amplitude anomalies (coloured circles, $m \cdot s^{-1}$) and the diurnal maximum seaward (blue vectors, $m \cdot s^{-1}$) and landward (red vectors, $m \cdot s^{-1}$) wind perturbation during austral summer (DJF) from 2011 to 2022 during eight different MJO phases at the (a) Brisbane radar and (b) Townsville radar. Black borders represent stations with results statistically significant at the 90% level using Student's *t* test. Times when the diurnal wind perturbation reaches its maximum are indicated in the right corner of each plot. [Colour figure can be viewed at wileyonlinelibrary.com]

only two phases that show low-level (850-hPa) westerly/southwesterly anomalies, but phase 1 exhibits much stronger wind speed anomalies (see Figure 10a). Natoli and Maloney (2023b) recently pointed out that a strong diurnal rainfall amplitude is more likely to occur on days with weak to moderate offshore low-level winds, which

promote a strong sea breeze circulation, and near to above average column moisture in the local environment. They also found that the transition from the suppressed to enhanced convection phase of intraseasonal variability tends to produce these favourable environmental conditions. Among the enhanced convection phases of the MJO (phases 4–6), the land–sea breeze generally decreases during phase 4 and increases during phase 6. This suggests that the variations in the strength of land–sea breeze circulation may contribute to the different rainfall patterns among the enhanced convection phases of the MJO (e.g., phase 4 versus phase 6) at the Brisbane radar. Sea breezes have also been highlighted as an important factor influencing hailstorm development on a local scale over southeast Queensland (Soderholm et al., 2017).

For Townsville (Figure 11b), the land–sea breeze is statistically weaker (negative anomalies) during phases 6 and 7, and stronger (positive anomalies) during phases 1–3 of the MJO. This is consistent with many previous studies over the Maritime Continent (Birch et al., 2016; Peatman et al., 2014; Short et al., 2019; Vincent & Lane, 2017; Wei et al., 2020) and northern Australia (Rauniyar & Walsh, 2016) stating that land–sea breeze tends to weaken during the enhanced convection phase and strengthen during the suppressed convection phase of the MJO. Given that land–sea breeze convergence is known to be a driver of local rainfall enhancement, this could help partly explain the enhanced rainfall over the ocean part of Townsville radar (see Figures 2b and 3b) during phases 1–3. Using the Met Office Unified Model simulations to understand the physical mechanisms behind offshore rainfall propagation over Sumatra, Peatman et al. (2023) highlighted the role of land breezes in driving rainfall offshore. They found that convection and precipitation occur over the mountain top in the late afternoon/early evening due to the sea breeze convergence and then propagate offshore at night at a similar speed of the land breeze density current. This suggests that the strong land breeze during phases 1–3 at the Townsville radar may be responsible for the enhanced rainfall signal with a morning rainfall peak over the ocean during these phases. In addition to having strong land–sea breeze circulation, phase 3 also exhibits the strongest low-level easterly anomalies (see Figure 10b), which coincide with the increased mean rainfall probability across the entire radar domain during this phase (see Figure 2b). Note that the easterly anomalies observed in the sounding data in phase 3 are relative to the prevailing background easterly trade wind regime, indicating enhanced onshore flow. This suggests that the strength of both the land–sea breeze circulation and the background winds may influence the extent to which rainfall can propagate. The stronger land–sea breeze circulation also helps explain the stronger diurnal precipitation variation during the suppressed convection phase of the MJO (e.g., phases 1–3) presented in the previous section.

5 | DISCUSSIONS AND CONCLUSIONS

Although previous studies have investigated the influences of the MJO on rainfall over many parts of Australia, how these impacts are modulated by local forcings has not been well understood. This study examines the variation of local rainfall with MJO phases in NE Australia using two modern S-band Doppler radars over the coastal area of north Queensland, where the rainfall signals are pronounced and often affected by the local circulations. The results demonstrate that at the local scale, there are notable variations in the MJO-scale modulation of rainfall. Importantly, although most locations show variation of rainfall with MJO phase, this variation is not necessarily in phase with the onset of the large-scale convective envelope of the MJO. The key findings are summarized below:

1. The variation of precipitation with the MJO over coastal regions of NE Australia exhibits both large-scale and local-scale influences. Daily rainfall probability generally increases during enhanced convection phases and decreases during suppressed convection phases of the MJO. However, there are some notable exceptions to this general notion in both Townsville and Brisbane radars. During suppressed MJO phases, when below-normal rainfall is expected, enhanced rainfall signals are also observed near high-terrain areas or over the ocean regions in both radar domains.
2. The variation of heavy-rainfall probability with MJO phases is generally similar to that of mean rainfall, consistent with previous studies (Dao et al., 2023; Wheeler et al., 2009). However, our results also indicate some differences in the responses of mean and heavy precipitation to the MJO at both radar sites, which were not reported in previous studies. For example, there is a statistically significant increase in rainfall probability exceeding the 90th percentile threshold, but no corresponding increase in the probability of rainfall exceeding the 67th percentile threshold in phase 5 over the oceanic part of the Brisbane radar.
3. The influence of the MJO on the diurnal rainfall cycle over coastal areas of NE Australia is spatially inhomogeneous and likely regulated by local forcings. Additionally, the impact of the MJO on diurnal rainfall characteristics (e.g., diurnal rainfall amplitude and timing) varies from phase to phase, particularly at the Brisbane radar. The largest diurnal amplitudes across the whole radar domains are found in the suppressed

MJO phases, but this is not the case everywhere. For example, enhanced diurnal cycles are found over land in some parts of the Townsville radar domain in phase 7. This suggests that instead of grouping MJO periods into enhanced and suppressed convection phases, each MJO period should be considered separately as it may have different local influences.

4. While stratiform rainfall occurs more frequently, convective rainfall predominantly contributes to the total precipitation at both radars. The MJO's impact on convective precipitation tends to be stronger and more statistically significant compared to its impact on stratiform precipitation over coastal areas of NE Australia.
5. The widespread increase in rainfall probability during the enhanced convection phases is likely due to an increase in both stratiform and convective rainfall. In contrast, the locally enhanced rainfall probability during certain suppressed convection MJO phases mainly results from an increase in convective rainfall at both radar sites.
6. During the enhanced convection phases of the MJO, widespread increased rainfall is consistent with the large-scale forcings associated with the MJO convection, but the factors influencing rainfall amount and type are different among those phases. In contrast, the enhanced precipitation signal during suppressed convection phases is likely codriven by mesoscale land–sea breezes, and their interaction with strong large-scale background wind and topography.

Our radar-based rainfall analysis strengthens the understanding from previous studies (Cowan et al., 2023; Dao et al., 2023; Marshall et al., 2021; Wheeler et al., 2009) that mean and heavy-rainfall probabilities generally increase during enhanced convection phases and decrease during suppressed convection phases of the MJO. Moreover, with a higher temporal and spatial resolution, this study further highlights the spatial inhomogeneity of the local rainfall response to the MJO. The locally reversed rainfall response to the MJO observed in this study highlights the importance of process-based understanding at small scales, such as city or farm scale, where rainfall responses may differ from the large-scale perspective. This is important for assessing the impact of climate change on precipitation at these scales and has potential value for water resource and agricultural management. Our results also show the different responses of mean and heavy rainfall to the MJO in certain phases, which were not reported in previous studies. Further analysis is needed to fully understand the reasons behind these discrepancies as well as behind some reversed local variation of precipitation with MJO phases. For example, high-resolution model (e.g., convective permitting models) data would be needed to unpack the full vertical structure of the atmosphere. In addition, previous studies have highlighted the impact of El Niño–Southern Oscillation (ENSO) on MJO itself (Watterson & Syktus, 2007; Wei & Ren, 2019), as well as on the MJO–rainfall relationship in tropical Australia (Cowan et al., 2023; Dao et al., 2023; Ghelani et al., 2017). Therefore, future research could further explore the impact of different ENSO states on the local rainfall response to the MJO using longer-period datasets.

The amplitude of diurnal precipitation variability in suppressed convection phases is generally larger than in enhanced convection phases of the MJO, consistent with previous studies in the Maritime Continent (Peatman et al., 2014; Rauniyar & Walsh, 2011; Vincent & Lane, 2016) and in NE Australia (Dao et al., 2023). The variation of diurnal precipitation amplitude with the MJO is likely associated with the change of both background and local winds, as well as changes to radiative forcing (Birch et al., 2016; Natoli & Maloney, 2023b; Peatman et al., 2014; Rauniyar & Walsh, 2016; Vincent & Lane, 2017; Wei et al., 2020). Using radar data and considering each MJO phase separately, this study further shows that diurnal precipitation characteristics associated with the MJO are inhomogeneous and regulated by local forcings. These findings help improve understanding of the timing and amplitude of short-duration rainfall extremes, which can cause flash flooding. Such extremes are projected to intensify over time in Australia (Jakob et al., 2020). Information on convective and stratiform precipitation enhances our understanding of the nature of precipitation over coastal areas of NE Australia. The contribution of convective and stratiform rainfall to total rainfall varies with MJO phases, suggesting that different processes are driving the local MJO rainfall response. These finding indicates that separately considering convective and stratiform processes is essential for better understanding intraseasonal precipitation variability. Additionally, these results are relevant to heavy-rainfall predictions and also to the question of how convective and stratiform rainfall processes will be modified in a warmer climate.

To the best of our knowledge, this is the first study to examine how the MJO interacts with local features in regulating rainfall and its diurnal cycle over coastal areas of NE Australia using high spatial and temporal resolution radar data. This study finds that the variation of rainfall with MJO phases exhibits both large-scale and local-scale influences. This suggests that to improve the intraseasonal prediction of heavy-rainfall events, numerical models need to capture both large-scale and local-scale geographical variations of rainfall. The findings are also crucial for quantifying numerical model biases on different spatial and temporal scales. Note that with only 11 DJF seasons, some MJO phases (e.g., phases 1, 8) have relatively small

sample sizes, which may affect the statistical significance of rainfall results during these phases. Although the areas of significant results are small in some plots, our results still clearly demonstrate the variation of rainfall during the enhanced and suppressed convection phases, as well as the geographical variation of MJO-associated rainfall pattern. For example, statistically significant rainfall variations are observed near the coast and high-terrain areas. These local variations are crucial for assessing rainfall at small scales and should not be ignored. Additionally, the consistent results across all plots highlight the MJO's influence on coastal rainfall over NE Australia. These findings will motivate future studies to examine the interactions between large-scale climate modes and local-scale forcings, and their influences on extreme events.

ACKNOWLEDGEMENTS

This work was funded by the Melbourne Research Scholarship, the Rowden White Scholarship, and the Australian Research Council (ARC) Centre of Excellence for the Weather of the 21st Century (CE230100012). Analysis was performed using the National Computing Infrastructure (NCI) National Facility. The authors thank Dr Jeremy Silver for insightful comments on the statistical aspects. Open access publishing facilitated by The University of Melbourne, as part of the Wiley - The University of Melbourne agreement via the Council of Australian University Librarians.

CONFLICT OF INTEREST STATEMENT

The authors have no conflicts of interest to declare.

DATA AVAILABILITY STATEMENT

The Australian Unified Radar Archive data level 2 dataset (Soderholm et al., 2022) is available at National Computational Infrastructure (NCI) under a CC4-BY-NC licence from https://doi.org/10.25914/JJWZ-0F13. Station wind data were obtained from the Australia Bureau of Meteorology. Daily upper-air soundings were downloaded from the University of Wyoming (https://weather.uwyo.edu/upperair/sounding.html). The Real-time Multivariate MJO (RMM) index was downloaded from the Australia Bureau of Meteorology (http://www.bom.gov.au/climate/mjo/) The codes can be made available by the corresponding author upon reasonable request.

ORCID

Thi Lan Dao https://orcid.org/0000-0003-2467-271X
C. L. Vincent https://orcid.org/0000-0001-5315-1644

REFERENCES

Alber, K., Zhou, L., Roundy, P.R. & Solimine, S.L. (2023) Influence of the Madden Julian oscillation on the diurnal cycles of convection and precipitation over Congo Basin. *Atmospheric Research*, 294, 106976. Available from: https://doi.org/10.1016/j.atmosres.2023.106967

Ayat, H., Evans, J.P., Sherwood, S.C. & Soderholm, J. (2023) An object-based climatology of precipitation systems in Sydney, Australia. *Climate Dynamics*, 60(5), 1669–1688. Available from: https://doi.org/10.1007/s00382-022-06404-z

Bai, H. (2021) Formation of nocturnal offshore rainfall near the west coast of Sumatra: land breeze or gravity wave? *Monthly Weather Review*, 149, 715–731. Available from: https://doi.org/10.1175/MWR-D-20-0179.1

Birch, C.E., Webster, S., Peatman, S.C., Parker, D.J., Matthews, A.J., Li, Y. et al. (2016) Scale interactions between the MJO and the Western maritime continent. *Journal of Climate*, 29(7), 2471–2492. Available from: https://doi.org/10.1175/JCLI-D-15-0557.1

Black, M.T. & Lane, T.P. (2015) An improved diagnostic for summertime rainfall along the eastern seaboard of Australia. *International Journal of Climatology*, 35(15), 4480–4492. Available from: https://doi.org/10.1002/joc.4300

Bretherton, C.S., Peters, M.E. & Back, L.E. (2004) Relationships between water vapor path and precipitation over the tropical oceans. *Journal of Climate*, 17, 1517–1528. Available from: https://doi.org/10.1175/1520-0442(2004)017,1517:RBWVPA.2.0.CO;2

Bui, H.X., Maloney, E.D., Short, E. & Riley Dellaripa, E.M. (2023) Diurnal cycle of wind speed and precipitation over the northern Australia coastal region: CYGNSS observations. *Geophysical Research Letters*, 50(8), e2023GL103005. Available from: https://doi.org/10.1029/2023GL103005

Chen, X., Zhang, F. & Zhao, K. (2016) Diurnal variations of land/sea breeze and its related precipitation over South China. *Journal of Geophysical Research: Atmospheres*, 73, 4793–4815. Available from: https://doi.org/10.1175/JAS-D-16-0106.1

Cowan, T., Wheeler, M.C., Alves, O., Narsey, S., Burgh-Day, C.d., Griffiths, M. et al. (2019) Forecasting the extreme rainfall, low temperatures, and strong winds associated with the northern Queensland floods of February 2019. *Weather and Climate Extremes*, 26, 100232. Available from: https://doi.org/10.1016/j.wace.2019.100232

Cowan, T., Wheeler, M.C. & Marshall, A.G. (2023) The combined influence of the Madden–Julian oscillation and El Niño–southern oscillation on Australian rainfall. *Journal of Climate*, 36(2), 313–334. Available from: https://doi.org/10.1175/JCLI-D-22-0357.1

Dahl, N.A., Shapiro, A., Potvin, C.K., Theisen, A., Gebauer, J.G., Schenkman, A.D. et al. (2019) High-resolution, rapid-scan dual-doppler retrievals of vertical velocity in a simulated supercell. *Journal of Atmospheric and Oceanic Technology*, 36(8), 1477–1500. Available from: https://doi.org/10.1175/JTECH-D-18-0211.1

Dao, T.L., Vincent, C.L. & Lane, T.P. (2023) Multiscale influences on rainfall in Northeast Australia. *Journal of Climate*, 36(17), 5989–6006. Available from: https://doi.org/10.1175/JCLI-D-22-0835.1

Davies, R. (2024) Tropical cyclone Jasper, Queensland, Australia - December 2023. *Emergency Management Service*.

Gabella, M. & Notarpietro, R. (2002) Ground clutter characterization and elimination in mountainous terrain. In: *Proceedings 2nd*

European conference on radar meteorology. Delft, The Netherlands: ERDA.

Ghelani, R.P.S., Oliver, E.C.J., Holbrook, N.J., Wheeler, M.C. & Klotzbach, P.J. (2017) Joint modulation of Intraseasonal rainfall in tropical Australia by the Madden-Julian oscillation and El Niño-southern oscillation. *Geophysical Research Letters*, 44(20), 10754–710761. Available from: https://doi.org/10.1002/2017GL075452

Goodwin, I.D. (2022) The Weather behind the Eastern Australian floods-the storm cluster from 23rd February to 2nd April. Risk frontiers, Briefing Note 464.

Hitchcock, S.M., Lane, T.P., Warren, R.A. & Soderholm, J.S. (2021) Linear rainfall features and their association with rainfall extremes near Melbourne, Australia. *Monthly Weather Review*, 149(10), 3401–3417. Available from: https://doi.org/10.1175/MWR-D-21-0007.1

Houze, R.A., Jr. (1997) Stratiform precipitation in regions of convection: a meteorological paradox. *Bulletin of the American Meteorological Society*, 78, 2179–2196. Available from: https://doi.org/10.1175/1520-0477(1997)078<2179>2.0.CO;2

Houze, R.A., Jr., Rasmussen, K.L., Zuluaga, M.D. & Brodzik, S.R. (2015) The variable nature of convection in the tropics and subtropics: a legacy of 16 years of the tropical rainfall measuring Mission satellite. *Reviews of Geophysics*, 53, 994–1021. Available from: https://doi.org/10.1002/2015RG000488

Huang, W.R., Hsu, H.H., Wang, S.Y. & Chen, J.P. (2015) Impact of atmospheric changes on the low-frequency variations of convective afternoon rainfall activity over Taiwan. *Journal of Geophysical Research: Atmospheres*, 120, 8743–8758. Available from: https://doi.org/10.1002/2015JD023568

Jakob, D., Hope, P., Osburn, L. & Smith, L. (2020) Short-duration, heavy rainfall is intensifying, but not everywhere, and not all the time: a literature review. In: *Bureau research report*. Australia: Bureau of Meteorology.

King, A.D., Alexander, L.V. & Donat, M.G. (2013) Asymmetry in the response of eastern Australia extreme rainfall to low-frequency Pacific variability. *Geophysical Research Letters*, 40, 2271–2277. Available from: https://doi.org/10.1002/grl.50427

Kumar, V.V., Protat, A., May, P.T., Jakob, C., Penide, G., Kumar, S. et al. (2013) On the effects of large-scale environment and surface types on convective cloud characteristics over Darwin, Australia. *Monthly Weather Review*, 141(4), 1358–1374. Available from: https://doi.org/10.1175/MWR-D-12-00160.1

Lestari, S., King, A., Vincent, C., Protat, A., Karoly, D. & Mori, S. (2022) Variability of Jakarta rain-rate characteristics associated with the Madden–Julian oscillation and topography. *Monthly Weather Review*, 150(8), 1953–1975. Available from: https://doi.org/10.1175/MWR-D-21-0112.1

Li, W., Zhang, F., Yu, Y., Iwabuchi, H., Shen, Z., Wang, G. et al. (2021) The semi-diurnal cycle of deep convective systems over eastern China and its surrounding seas in summer based on an automatic tracking algorithm. *Climate Dynamics*, 56(1-2), 357–379. Available from: https://doi.org/10.1007/s00382-020-05474-1

Ling, J., Zhang, C., Joyce, R., Xie, P.-p. & Chen, G. (2019) Possible role of the diurnal cycle in land convection in the barrier effect on the MJO by the maritime continent. *Geophysical Research Letters*, 46(5), 3001–3011. Available from: https://doi.org/10.1029/2019GL081962

Lopez-Bravo, C., Vincent, C.L., Huang, Y. & Lane, T.P. (2023) The diurnal cycle of rainfall and deep convective clouds around Sumatra and the associated MJO-induced variability during austral summer in Himawari-8. *Journal of Geophysical Research: Atmospheres*, 128(22), e2023JD039132. Available from: https://doi.org/10.1029/2023JD039132

Louf, V., Protat, A., Warren, R.A., Collis, S.M., Wolff, D.B., Raunyiar, S. et al. (2019) An integrated approach to weather radar calibration and monitoring using ground clutter and satellite comparisons. *Journal of Atmospheric and Oceanic Technology*, 36(1), 17–39. Available from: https://doi.org/10.1175/JTECH-D-18-0007.1

Love, B.S., Matthews, A.J. & Lister, G.M.S. (2011) The diurnal cycle of precipitation over the maritime continent in a high-resolution atmospheric model. *Quarterly Journal of the Royal Meteorological Society*, 137(657), 934–947. Available from: https://doi.org/10.1002/qj.809

Madden, R.A. & Julian, P.R. (1971) Detection of a 40–50 Day oscillation in the zonal wind in the tropical Pacific. *Journal of Atmospheric Sciences*, 28(5), 702–708. Available from: https://doi.org/10.1175/1520-0469(1971)028<0702:DOADOI>2.0.CO;2

Madden, R.A. & Julian, P.R. (1972) Description of global-scale circulation cells in the tropics with a 40–50 Day period. *Journal of Atmospheric Sciences*, 29(6), 1109–1123. Available from: https://doi.org/10.1175/1520-0469(1972)029<1109:DOGSCC>2.0.CO;2

Marshall, A.G., Hendon, H.H. & Hudson, D. (2021) Influence of the Madden-Julian oscillation on multiweek prediction of Australian rainfall extremes using the ACCESS-S1 prediction system. *Journal of Southern Hemisphere Earth Systems Science*, 71(2), 159–180. Available from: https://doi.org/10.1071/ES21001

Matthews, A.J., Hoskins, B.J. & Masutani, M. (2004) The global response to tropical heating in the Madden–Julian oscillation during the northern winter. *Quarterly Journal of the Royal Meteorological Society*, 130(601), 1991–2011. Available from: https://doi.org/10.1256/qj.02.123

May, P.T., Long, C.N. & Protat, A. (2012) The diurnal cycle of the boundary layer, convection, clouds, and surface radiation in a coastal monsoon environment (Darwin, Australia). *Journal of Climate*, 25(15), 5309–5326. Available from: https://doi.org/10.1175/JCLI-D-11-00538.1

Miller, S.T.K., Keim, B.D., Talbot, R.W. & Mao, H. (2003) Sea breeze: structure, forecasting, and impacts. *Reviews of Geophysics*, 41, 1011–1048. Available from: https://doi.org/10.1029/2003RG000124

Muhammad, F.R., Lubis, S.W. & Setiawan, S. (2020) Impacts of themadden-Julian oscillation on precipitation extremes in Indonesia. *International Journal of Climatology*, 41, 1970–1984. Available from: https://doi.org/10.1002/joc.6941

Natoli, M.B. & Maloney, E.D. (2023a) The tropical diurnal cycle under varying states of the monsoonal background wind. *Journal of the Atmospheric Sciences*, 80(1), 235–258. Available from: https://doi.org/10.1175/jas-d-22-0045.1

Natoli, M.B. & Maloney, E.D. (2023b) Environmental controls on the tropical Island diurnal cycle in the context of intraseasonal variability. *Journal of Climate*, 36, 7465–7485. Available from: https://doi.org/10.1175/JCLI-D-22-0824.1

Oh, J.-H., Kim, K.-Y. & Lim, G.-H. (2012) Impact of MJO on the diurnal cycle of rainfall over the western maritime continent in the

austral summer. *Climate Dynamics*, 38(5), 1167–1180. Available from: https://doi.org/10.1007/s00382-011-1237-4

Peatman, S.C., Birch, C.E., Schwendike, J., Marsham, J.H., Dearden, C., Webster, S. et al. (2023) The role of density currents and gravity waves in the offshore propagation of convection over Sumatra. *Monthly Weather Review*, 151, 1757–1777.

Peatman, S.C., Matthews, A.J. & Stevens, D.P. (2014) Propagation of the Madden–Julian oscillation through the maritime continent and scale interaction with the diurnal cycle of precipitation. *Quarterly Journal of the Royal Meteorological Society*, 140(680), 814–825. Available from: https://doi.org/10.1002/qj.2161

Pepler, A.S., Dowdy, A.J., van Rensch, P., Rudeva, I., Catto, J.L. & Hope, P. (2020) The contributions of fronts, lows and thunderstorms to southern Australian rainfall. *Climate Dynamics*, 55(5), 1489–1505. Available from: https://doi.org/10.1007/s00382-020-05338-8

Pourasghar, F., Oliver, E.C. & Holbrook, N.J. (2019) Modulation of wet-season rainfall over Iran by the Madden–Julian oscillation, Indian Ocean dipole and El Niño–southern oscillation. *International Journal of Climatology*, 39, 4029–4040. Available from: https://doi.org/10.1002/joc.6057

Powell, S.W. & Houze, R.A., Jr. (2013) The cloud population and onset of the Madden-Julian oscillation over the Indian Ocean during DYNAMO-AMIE. *Journal of Geophysical Research: Atmospheres*, 118, 11,979–11,995. Available from: https://doi.org/10.1002/2013JD020421

Qian, J.-H. (2020) Mechanisms for the dipolar patterns of rainfall variability over large islands in the maritime continent associated with the Madden–Julian oscillation. *Journal of the Atmospheric Sciences*, 77(6), 2257–2278. Available from: https://doi.org/10.1175/JAS-D-19-0091.1

Rauniyar, S.P. & Walsh, K.J.E. (2011) Scale interaction of the diurnal cycle of rainfall over the maritime continent and Australia: influence of the MJO. *Journal of Climate*, 24(2), 325–348. Available from: https://doi.org/10.1175/2010JCLI3673.1

Rauniyar, S.P. & Walsh, K.J.E. (2016) Spatial and temporal variations in rainfall over Darwin and its vicinity during different large-scale environments. *Climate Dynamics*, 46(3), 671–691. Available from: https://doi.org/10.1007/s00382-015-2606-1

Raut, B.A., Louf, V., Gayatri, K., Murugavel, P., Konwar, M. & Prabhakaran, T. (2020) A multiresolution technique for the classification of precipitation echoes in radar data. *IEEE Transactions on Geoscience and Remote Sensing*, 58(8), 5409–5415. Available from: https://doi.org/10.1109/TGRS.2020.2965649

Rowe, A.K., Houze Jr, R.A., Brodzik, S. & Zuluaga, M.D. (2019) The diurnal and microphysical characteristics of MJO rain events during DYNAMO. *Journal of the Atmospheric Sciences*, 76(7), 1975–1988. Available from: https://doi.org/10.1175/JAS-D-18-0316.1

Schreck, C.J., III. (2021) Global survey of the MJO and extreme precipitation. *Geophysical Research Letters*, 48(19), e2021GL094691. Available from: https://doi.org/10.1029/2021GL094691

Shen, L., Zhao, C., Ma, Z., Li, Z., Li, J. & Wang, K. (2019) Observed decrease of summer sea–land breeze in Shanghai from 1994 to 2014 and its association with urbanization. *Atmospheric Research*, 227, 198–209. Available from: https://doi.org/10.1016/j.atmosres.2019.05.007

Short, E., Vincent, C.L. & Lane, T.P. (2019) Diurnal cycle of surface winds in the maritime continent observed through satellite Scatterometry. *Monthly Weather Review*, 147(6), 2023–2044. Available from: https://doi.org/10.1175/MWR-D-18-0433.1

Smith, M., Poggio, M.J., Thompson, M. & Collier, A. (2014) The economics of pesticide management practices on sugarcane farms: final synthesis report. In: *Department of agriculture*. Queensland. Final Report, Brisbane: Fisheries and Forestry (DAFF), p. 54.

Soderholm, J., Louf, V., Brook, J., Protat, A. & Warren, R. (2022) Australian operational weather radar level 2 dataset. In: *National Computing Infrastructure*. Australia: National Computational Infrastructure (NCI). Available from: https://doi.org/10.25914/JJWZ-0F13

Soderholm, J., McGowan, H.A., Richter, H., Walsh, K., Weckwerth, T.M. & Coleman, M. (2016) The coastal convective interactions experiment (CCIE): understanding the role of sea breezes for hailstorm hotspots in eastern Australia. *Bulletin of the American Meteorological Society*, 97, 1687–1698. Available from: https://doi.org/10.1175/BAMS-D-14-00212.1

Soderholm, J.S., McGowan, H., Richter, H., Walsh, K., Weckwerth, T.M. & Coleman, M. (2017) An 18-year climatology of hailstorm trends and related drivers across southeast Queensland, Australia. *Quarterly Journal of the Royal Meteorological Society*, 143, 1123–1135. Available from: https://doi.org/10.1002/qj.2995

Twomey, C.R. & Kiem, A.S. (2021) Australian rainfall variability—why is the eastern seaboard of Australia different to the rest of Australia and also internally inhomogeneous. *International Journal of Climatology*, 41(10), 5051–5071. Available from: https://doi.org/10.1002/joc.7116

Vincent, C.L. & Lane, T.P. (2016) Evolution of the diurnal precipitation cycle with the passage of a Madden–Julian oscillation event through the maritime continent. *Monthly Weather Review*, 144(5), 1983–2005. Available from: https://doi.org/10.1175/MWR-D-15-0326.1

Vincent, C.L. & Lane, T.P. (2017) A 10-year austral summer climatology of observed and modeled Intraseasonal, mesoscale, and diurnal variations over the maritime continent. *Journal of Climate*, 30, 3807–3828. Available from: https://doi.org/10.1175/jcli-d-16-0688.1

Vincent, C.L. & Lane, T.P. (2018) Mesoscale variation in diabatic heating around Sumatra, and its modulation with the Madden–Julian oscillation. *Monthly Weather Review*, 146(8), 2599–2614. Available from: https://doi.org/10.1175/MWR-D-17-0392.1

Vincent, C.L., Lane, T.P. & Wheeler, M.C. (2016) A local index of maritime continent intraseasonal variability based on rain-rates over the land and sea. *Geophysical Research Letters*, 43(17), 9306–9314. Available from: https://doi.org/10.1002/2016GL069987

Watterson, I.G. & Syktus, J. (2007) The influence of air–sea interaction on the Madden–Julian oscillation: the role of the seasonal mean state. *Climate Dynamics*, 28, 703–722. Available from: https://doi.org/10.1007/s00382-006-0206-9

Wei, Y., Pu, Z. & Zhang, C. (2020) Diurnal cycle of precipitation over the maritime continent under modulation of MJO: perspectives from cloud-permitting scale simulations. *Journal of Geophysical*

Research: Atmospheres, 125(13), e2020JD032529. Available from: https://doi.org/10.1029/2020JD032529

Wei, Y. & Ren, H.-L. (2019) Modulation of ENSO on fast and slow MJO modes during boreal winter. *Journal of Climate*, 32, 7483–7506. Available from: https://doi.org/10.1175/JCLI-D-19-0013.1

Wheeler, M.C. & Hendon, H.H. (2004) An all-season real-time multivariate MJO index: development of an index for monitoring and prediction. *Monthly Weather Review*, 132(8), 1917–1932. Available from: https://doi.org/10.1175/1520-0493(2004)132<1917:AARMMI>2.0.CO;2

Wheeler, M.C., Hendon, H.H., Cleland, S., Meinke, H. & Donald, A. (2009) Impacts of the Madden–Julian oscillation on Australian rainfall and circulation. *Journal of Climate*, 22, 1482–1498. Available from: https://doi.org/10.1175/2008JCLI2595.1

SUPPORTING INFORMATION

Additional supporting information can be found online in the Supporting Information section at the end of this article.

How to cite this article: Dao, T.L., Vincent, C.L., Huang, Y. & Soderholm, J.S. (2025) Modulations of local rainfall in northeast Australia associated with the Madden–Julian oscillation during austral summer. *Quarterly Journal of the Royal Meteorological Society*, e4995. Available from: https://doi.org/10.1002/qj.4995